Evaluating the importance of street trees and their parameters for urban canopy model performance: Model updates and machine learning

Kyeongjoo Park [a], Jong-Jin Baik [a, *], Young-Hee Ryu [b]

[a] *School of Earth and Environmental Sciences, Seoul National University, Seoul 08826, South Korea*

[b] *Department of Atmospheric Sciences, Yonsei University, Seoul 03722, South Korea*

Preprint Statement:

This is a non-peer-reviewed preprint submitted to EarthArXiv. This work has been submitted to Urban Climate.

[*] Corresponding author.

E-mail address: jjbaik@snu.ac.kr (J.-J. Baik).

ABSTRACT

In this study, the effects of street trees on the performance of an urban canopy model (UCM) and how the UCM sensitively responds to tree-related parameters compared with urban thermal parameters are examined. For this, a single-layer UCM is extended to represent street trees within urban canyons and multi-objective parameter optimizations and a global sensitivity analysis are conducted with the aid of machine learning (ML) technique. Including street trees markedly improves the simulation performances of net radiation, sensible heat flux, and latent heat flux at both dense and vegetated urban sites, substantially reducing their systematic errors. Moreover, including street trees reduces the trade-off between the simulation performances of net radiation and sensible heat flux. At the dense urban site, the simulation performances of net radiation and sensible heat flux are the most sensitive to roof albedo while that of latent heat flux is the most sensitive to tree fraction. At the vegetated urban site, the tree-related parameters are the most influential for the simulation performances of all the three energy fluxes. This study emphasizes the importance of street trees in better simulating urban surface energy balance and presents an ML-based framework for efficient parameter optimization and sensitivity analysis.

Keywords: Urban canopy model, Street tree, Urban parameter, Optimization, Sensitivity, Machine learning

1. Introduction

As urban areas have been expanding globally (Seto et al., 2011; Hanberry, 2023), it is of growing importance to better understand and predict urban weather and climate (Hamdi et al., 2020; Qian et al., 2022). To appropriately represent and simulate urban impacts on the atmosphere, a number of urban canopy models (UCMs) have been developed and implemented in weather/climate models (e.g., Masson, 2000; Kusaka et al., 2001; Martilli et al., 2002; Oleson et al., 2008; Ryu et al., 2011). UCMs consider urban canyons constituted by building walls and roads and simulate the energy and water exchanges between urban surfaces and the adjacent air, enabling a realistic representation of complex land–atmosphere interactions appearing in urban areas (Jandaghian and Berardi, 2020). The implementation of UCMs has led to the successful simulations of diverse urban weather and climate phenomena such as urban heat islands, urban dry islands, and urban-induced precipitation modifications (e.g., Kusaka et al., 2012; Hu et al., 2024; Zhou et al., 2024b).

As UCMs have emerged as an essential component for high-resolution urban weather/climate modeling (Ching, 2013), the performances of various UCMs have been extensively evaluated and substantial model improvements have been made (Grimmond et al., 2010; Grimmond et al., 2011; Jongen et al., 2024; Lipson et al., 2024). In particular, many researchers have focused on representing urban vegetation within urban canyons, and it has been revealed that including street trees substantially contributes to better simulating urban surface energy fluxes and urban canyon air temperature (Krayenhoff et al., 2014; Ryu et al., 2016; Krayenhoff et al., 2020; Meili et al., 2020; Mussetti et al., 2020; Wang et al., 2021). Ryu et al. (2016) represented two rows of street trees in a UCM and showed that the inclusion of street trees improves the performances in simulating latent heat flux and canyon air temperature at both urban and suburban sites. Meili et al. (2020) developed an urban ecohydrological model which explicitly represents street trees and revealed that the model better performs than other UCMs in simulating surface energy fluxes, especially at a tropical urban site. Wang et al. (2021) incorporated a single row of street trees in a UCM and showed that the inclusion of street trees leads to marked improvements in the performances in simulating surface energy fluxes and canyon air temperature.

Since street trees require additional tree-related input parameters and intricately interact with the ground and buildings (Meili et al., 2021), their inclusion in UCMs appears to make it challenging to find an optimized parameter set for a specific urban site and to substantially affect the UCM's sensitivities to individual parameters. Most previous studies conducted parameter optimization and/or examined parameter sensitivities using UCMs without representing street trees (e.g., Loridan et al., 2010; Wang et al., 2011; Yang and Wang, 2014; Zhao et al., 2014; Nemunaitis-Berry et al., 2017; Tsiringakis et al., 2019; Tsiringakis et al., 2020; Ao and Zhang, 2022). Loridan et al. (2010) evaluated the performance of a UCM and examined parameter sensitivities through a multi-objective optimization method. They found that the UCM is highly sensitive to roof-related parameters while it exhibits low sensitivities to road-related parameters. Wang et al. (2011) quantified the effects of parameter uncertainties on the performance of a UCM through an advanced Monte Carlo approach and showed that the uncertainties in urban morphological parameters highly affect the simulated surface energy fluxes. Ao and Zhang (2022) conducted parameter optimization and sensitivity analysis using a UCM and showed that the net radiation and sensible heat flux are highly sensitive to roof and wall albedos.

Although several previous studies have investigated the individual sensitivities of model outputs to tree-related parameters using UCMs with representing street trees (e.g., Ryu et al., 2016; Krayenhoff et al., 2020; Wang et al., 2021), how sensitive a UCM is to tree-related parameters relative to other urban parameters has not yet been rigorously investigated. The use of a global sensitivity analysis method is necessary to investigate this with considering complex interrelationships among tree-related and other urban parameters (Song et al., 2015) but requires numerous UCM simulations with different parameter sets, resulting in large computational costs. Regarding this, the machine learning (ML) technique is an efficient tool to well capture the nonlinear relationships between model parameters and outputs and generate a large number of surrogate predictions within a very short computational time (Zhao et al., 2023). The ML-based surrogate modeling has been widely conducted in the field of urban weather/climate modeling (e.g., Lu et al., 2022; Hora and Giometto, 2024; Zhao et al., 2024). Moreover, the ML technique can also be used for parameter optimization (Li et al., 2022; Zhang et al., 2024), which enables a more robust evaluation of the effects of including street trees on UCM performances for a specific urban site.

This study aims to evaluate how the inclusion of street trees affects the performance of a UCM and examine how tree-related parameters are influential to UCM simulations compared with other urban thermal parameters. For this, the Seoul National University UCM (SNUUCM), a single-layer UCM developed by Ryu et al. (2011), is updated to incorporate in-canyon street trees and their associated physical processes. The SNUUCM possesses a distinct feature that simulates the physical processes occurring at the two facing building walls individually, thereby well capturing the thermal contrast between them (Ryu et al., 2011). The SNUUCM exhibits comparable performances in simulating surface energy fluxes compared with other various urban land surface models (Grimmond et al., 2010; Grimmond et al., 2011; Lipson et al., 2024). However, the representation of urban vegetation effects relies entirely on the Noah land surface model (Chen and Dudhia, 2001) coupled through a tile approach, which needs an improvement for representing in-canyon vegetation and its interactions with the ground and buildings. To robustly evaluate street trees' effects on model performance, parameter optimizations both in the presence and absence of street trees are conducted using a multi-objective genetic algorithm and the performances in simulating surface energy fluxes are compared. To compare the sensitivities of simulated urban surface energy fluxes to tree-related parameters with those to other urban thermal parameters, a global sensitivity analysis method is employed. For the efficient implementation of both parameter optimization and sensitivity analysis, ML models to predict the performances in simulating surface energy fluxes from the given input parameters are constructed. The overall workflow of this study is presented in Fig. 1.

2. Methods

2.1. Updates to the SNUUCM

In this subsection, the main updates made to the SNUUCM are described. Through the updates, the SNUUCM is extended to represent street trees within urban canyons as well as the vegetated ground where street trees are situated and the associated soil hydrological processes occur (Fig. 2). In this study, the updated version of the SNUUCM is called the SNUUCM-Tree. Following Ryu et al. (2016), two rows of street trees which are equidistant from the adjacent wall and whose crowns are circular in a two-dimensional plane are considered and it is assumed that the trunks of street trees have negligible influence on the radiative processes within urban canyons. The calculations of direct shortwave radiation incident on street trees and shadow lengths due to walls and street trees follow the method of Ryu et al. (2016), whereas, given the SNUUCM's feature, the direct shortwave radiation for walls is totally assigned to the sunlit walls and the direct shortwave radiation for the shaded walls is set to zero.

The formulations of the major physical processes which are newly added or modified to represent street trees are summarized in Tables 1 and 2. The view factors in the presence of street trees are difficult to be analytically formulated and thus are commonly obtained through the Monte Carlo ray tracing method (Wang, 2014). For the practical estimation of view factors under various configurations of urban canyons and street trees, the multiple linear regression equations obtained by Ryu et al. (2016) through the Monte Carlo ray tracing simulations are used with some modifications (Eqs. (1)–(11)): To account for the view factors from the ground (street trees) to either the sunlit walls or shaded walls, the factor 0.5 is multiplied in Eq. (3) (Eq. (9)), and consequently the factor 2 is multiplied to F_{tw} in Eq. (11). As in the SNUUCM, three-time reflections of shortwave radiation and one-time reflection of longwave radiation are considered, while the reflections occur among the ground, sunlit and shaded walls, and street trees and the areal factors are considered in calculating net radiation for each in-canyon surface in the presence of street trees (Eqs. (12) and (13)). Note that the effective albedo, emissivity, and temperature are used for the ground when the reflections and radiation trapping are calculated. Finally, the net shortwave and longwave radiations for the impervious ground (roads), vegetated ground, and sunlit and shaded walls are calculated as the weighted averages using the fraction of urban canyons with street trees (hereafter, tree fraction) (Eqs. (14) and (15)).

As in several other UCMs with street trees (e.g., Ryu et al., 2016; Wang et al., 2021), the leaf sensible heat flux is calculated using the leaf boundary-layer resistance whose formulation is empirically obtained by Landsberg and Powell (1973) (Eq. (16)) and the leaf latent heat flux is calculated through the Penman-Monteith equation given in Green (1993) (Eq. (17)). For the vegetated ground, the sensible heat flux is calculated through the Monin-Obukhov similarity theory as for the impervious ground (Ryu et al., 2011) and the latent heat flux is calculated following the method of Wang et al. (2013). The soil hydrological processes including root-water uptake are represented in the same way as those in Ryu et al. (2016), four soil layers being considered. The prognostic equations for canyon air temperature and humidity are modified to incorporate the effects of the vegetated ground and street trees (Eqs. (18) and (19)), and the leaf temperature is prognosed through Eq. (20), the leaf heat capacity being set to 640 J m^{-2} K^{-1} (Ryu et al., 2016).

Due to the inclusion of in-canyon vegetation, several additional input parameters are incorporated into the SNUUCM-Tree. The key tree-related parameters include the tree fraction, tree-crown radius, tree height, tree-to-wall distance, leaf area index (LAI), leaf albedo, and leaf emissivity. The remaining additional input parameters are mainly related to the vegetated ground, including its fraction, albedo, emissivity, heat capacity, thermal conductivity, roughness lengths, and LAI.

2.2. Machine learning technique and observational data

In this subsection, the ML models and observational data utilized for the analyses are described. For use in both parameter optimization and sensitivity analysis of the simulation performances of surface energy fluxes, the ML models are designed to predict the root mean square errors (RMSEs) of net radiation ($RMSE_{RN}$), sensible heat flux ($RMSE_{SH}$), and latent heat flux ($RMSE_{LH}$) simulated by the SNUUCM-Tree against observations from given input parameters. The six tree-related parameters and nineteen urban thermal parameters are selected for optimization and sensitivity analysis and are presented in Table 3, being used as the predictor variables for the ML models. The ML models are constructed using the eXtreme Gradient Boosting (XGBoost) algorithm (Chen and Guestrin, 2016) which is based on an ensemble of decision trees implemented within the gradient boosting framework. XGboost is well known for its capability to well capture nonlinear relationships between target and predictor variables and its explainability (Başağaoğlu et al., 2022) and is therefore widely used for prediction and/or attribution analysis in the related fields (e.g., Shao et al., 2023; Tanoori et al., 2024).

The Basel UrBan Boundary Layer Experiment (BUBBLE) campaign (Rotach et al., 2005) dataset is used as observational data for constructing the ML models and evaluating the performance of the SNUUCM-Tree. During the summer intensive observation period between 10 June and 10 July in 2002, flux tower measurements were conducted at seven sites in Basel, Switzerland (Christen and Vogt, 2004). Among these sites, the Basel-Sperrstrasse site, which represents a dense urban area (Rotach et al., 2005), is adopted for the main analyses. To generate the training dataset of the ML models, the offline SNUUCM-Tree simulations are conducted for the Basel-Sperrstrasse site with various combinations of the values of the 25 selected input parameters. For each simulation, the values of the 25 selected input parameters are sampled within their respective sampling ranges (Table 3). The Sobol' sequence (Sobol', 1967) and Latin hypercube sampling (McKay et al., 1979) are employed to make the values of the 25 input parameters in the training dataset be nearly uniformly distributed within the parameter space. The integration period is from 0000 LST 9 June to 0000 LST 10 July 2002 with a one-day spin-up period during which the same meteorological forcing as that on the following day is applied. $RMSE_{RN}$, $RMSE_{SH}$, and $RMSE_{LH}$ are obtained for the remaining 30-day analysis period, therefore each simulation yielding one training data which consists of a pair of predictor variables (the 25 input parameters) and target variables (the three RMSEs). Based on Christen and Vogt (2004), H, W, f_{vg}, and normalized roof width are set to 14.6 m, 11.2 m, 0.35, and 0.54, respectively. The ratio of momentum roughness length to heat roughness length is set to 10 (Ryu et al., 2011), the tree-to-wall distance is set to be a_t plus 1.5 m, and the initial soil moisture is set to 0.28 m^3 m^{-3} in the top soil layer and 0.35 m^3 m^{-3} in the bottom soil layer. As a result, total 46,153 generated data are used for training the ML models.

Using the generated data, the ML models are trained to learn the relationships between the selected 25 input parameters and RMSEs ($RMSE_{RN}$, $RMSE_{SH}$, and $RMSE_{LH}$) for the Basel-Sperrstrasse site. The optimal combination of hyperparameters for the ML models, including the number of decision trees, maximum tree depth, and learning rate, is explored using Optuna (Akiba et al., 2019), and the values of hyperparameters adopted are listed in Table S1. The prediction performances of the trained ML models are evaluated using additional 8,145 data generated from the offline SNUUCM-Tree simulations (Fig. 3). The ML models well reproduce $RMSE_{RN}$, $RMSE_{H}$, and $RMSE_{LE}$ obtained from the SNUUCM-Tree simulations for the Basel-Sperrstrasse site using the given selected input parameters. For all the three RMSEs, the coefficients of determination (R^2) between the ML model predictions and SNUUCM-Tree simulations are higher than 0.96 and the mean absolute errors (MAEs) of the ML model predictions are lower than 1.5 W m^{-2} against the SNUUCM-Tree simulations. Therefore, the constructed ML models appear to exhibit sufficient performances to serve as reliable surrogate tools for both parameter optimization and sensitivity analysis.

2.3. Multi-objective parameter optimization

To conduct the optimization of the selected input parameters, the Non-dominated Sorting Genetic Algorithm III (NSGA-III) (Deb and Jain, 2013) is adopted. The genetic algorithms, which mimic biological evolutions, are widely used for parameter optimization when there exist multiple, potentially conflicting, objective functions to be minimized or maximized simultaneously (e.g., Li et al., 2022; Werth and Buckley, 2022). The genetic algorithms generate random populations (parameter sets) and evaluate them against objective functions. Then, populations in the next generation are produced through the selection, crossover, and mutation. Iterating the evaluation and evolution, the algorithms find better solutions in the objective space (Katoch et al., 2021). Since the simultaneous minimization or maximization of multiple objective functions is performed, the genetic algorithms identify the Pareto solutions for which no other solution is better in terms of all objective functions (Sharma and Kumar, 2022). NSGA-III is a suitable algorithm for multi-objective parameter optimization (Zhou et al., 2024a) and has a distinct feature that a set of predefined reference directions is used to make the solutions be well spread across the objective space (Deb and Jain, 2013).

Using the NSGA-III algorithm, the multi-objective optimization of the selected input parameters is conducted for both cases with and without street trees (hereafter, Tree-on case and Tree-off case, respectively). In the Tree-off case, the tree fraction is fixed to zero, only ground vegetation being considered. For both cases, $RMSE_{RN}$, $RMSE_{SH}$, and $RMSE_{LH}$ are used as the objective functions to be minimized. The ranges of the optimized parameters are the same as those presented in Table 3. The number of populations in each generation is 528, and total 500 generations are considered. The objective functions for a given population (parameter set) are evaluated using the ML models (subsection 2.2), enabling the optimization to be completed with very low computational costs. As a result, total 274 and 346 Pareto-optimal parameter sets are identified in the Tree-on and Tree-off cases, respectively.

2.4. Sensitivity analysis

To compare the sensitivities of the SNUUCM-Tree to the tree-related parameters with those to the urban thermal parameters, the global sensitivity analysis is conducted using the Sobol' method (Sobol', 2001). The Sobol' method is one of the most widely used variance-based global sensitivity analysis methods in which the total variance of an output is decomposed into the contributions of input parameters (Van Stein et al., 2022). Compared with local sensitivity analysis methods such as the one-at-a time method, the Sobol' method has the advantage of quantifying both the individual and interaction effects of input parameters (Tian, 2013). For a function Y determined by n input parameters, the variance of Y is decomposed into the variances associated with the individual effects and interaction effects of input parameters as follows:

$$V(Y) = \sum_{i} V_i + \sum_{i<j} V_{ij} + \cdots + V_{1 \ldots n} \tag{21}$$

Here, $V(Y)$ is the variance of Y and i and j are the indices indicating each of n input parameters. The individual (first-order) effect and total effect of an input parameter are, respectively, quantified as

$$S_i = \frac{V_{X_i}(E_{X_{\sim i}}(Y \mid X_i))}{V(Y)} \tag{22}$$

$$S_{T_i} = 1 - \frac{V_{X_{\sim i}}(E_{X_i}(Y \mid X_{\sim i}))}{V(Y)} \tag{23}$$

where S_i and S_{Ti} are, respectively, the first-order and total-order Sobol' indices, X_i and $X_{\sim i}$ are, respectively, i-th input parameter and all input parameters except i-th input parameter, and E is the expectation. The numerator in the right-hand side of Eq. (22) indicates the variance of the conditional mean of Y given X_i, and that of Eq. (23) indicates the variance of the conditional mean of Y given $X_{\sim i}$. The interaction effect associated with i-th input parameter can be obtained by taking the difference between S_i and S_{Ti}. The input parameters exhibiting larger Sobol' indices are considered to be more sensitive parameters. Practically, the quantification of the Sobol' indices requires numerous Monte Carlo simulations (Sobol', 2001). To quantify the Sobol' indices for each of the 25 selected input parameters, total 884736 ML model simulations are conducted with the parameters being randomly sampled within their respective ranges (Table 3).

Note that we additionally construct the ML models for the Basel-Spalenring site (Table S1 and Fig. S1) which represents a vegetated urban area (Rotach et al., 2005) and perform parameter optimization and sensitivity analysis for this site in the same way. This is to investigate whether the effects of street trees on the performance of the SNUUCM-Tree and the sensitivities to the tree-related and urban thermal parameters significantly differ depending on the degree of urban vegetation.

3. Results and discussion

3.1. Effects of including street trees on model performance

To examine the effects of including street trees on the performance of the SNUUCM-Tree, the RMSEs of surface energy fluxes in the Tree-on and Tree-off cases are compared. For analysis, the total RMSE ($RMSE_{TOT}$) is additionally calculated as the sum of $RMSE_{RN}$, $RMSE_{SH}$, and $RMSE_{LH}$. Fig. 4 shows the box plots of $RMSE_{TOT}$, $RMSE_{RN}$, $RMSE_{SH}$, and $RMSE_{LH}$ obtained from the SNUUCM-Tree simulations with the Pareto-optimal parameter sets in the Tree-on and Tree-off cases. The inclusion of street trees leads to a substantial reduction in $RMSE_{TOT}$, the mean $RMSE_{TOT}$ being 74.8 W m^{-2} in the Tree-on case and 121.1 W m^{-2} in the Tree-off case (Fig. 4). It is also evidently seen that the variability of $RMSE_{TOT}$ among the Pareto-optimal parameter sets is much smaller in the Tree-on case than in the Tree-off case. The interquartile range of $RMSE_{TOT}$ in the Tree-on case is only 1.2 W m^{-2}, while that in the Tree-off case is 11.4 W m^{-2}. These results indicate that the inclusion of street trees not only significantly raises the maximum achievable performances in simulating surface energy fluxes but also enables a more robust identification of optimal input parameters. The substantial reduction in $RMSE_{TOT}$ due to the inclusion of street trees results from the reductions in all $RMSE_{RN}$, $RMSE_{SH}$, and $RMSE_{LH}$. Compared with the Tree-off case, the mean $RMSE_{RN}$, $RMSE_{SH}$, and $RMSE_{LH}$ in the Tree-on case are smaller by 17.0 W m^{-2}, 13.0 W m^{-2}, and 16.3 W m^{-2}, respectively, the improvement being more pronounced in simulating net radiation and latent heat flux than in simulating sensible heat flux. In the Tree-off case, the variabilities of $RMSE_{RN}$ and $RMSE_{SH}$ among the Pareto-optimal parameter sets are pronounced with their interquartile ranges being 15.3 W m^{-2} and 8.3 W m^{-2}, respectively. This implies the difficulty in achieving robust improvements particularly in the simulations of net radiation and sensible heat flux without including street trees. Meanwhile, in the Tree-on case, the variabilities of all $RMSE_{RN}$, $RMSE_{SH}$, and $RMSE_{LH}$ among the Pareto-optimal parameter sets are very small, their interquartile ranges being smaller than 1.2 W m^{-2}.

Fig. 5 shows the probability density functions (PDFs) of the 25 input parameters within the Pareto-optimal sets in the Tree-on and Tree-off cases. Compared with the Tree-off case, the PDFs of the majority of the urban thermal parameters (14 out of 19) in the Tree-on case exhibit much more distinct peaks (Fig. 5). For the PDFs of the tree-related parameters in the Tree-on case as well, clear peaks are overall found. These results also show that the inclusion of street trees facilitates finding an optimal parameter set to improve the simulations of all the three energy fluxes for the site.

How the inclusion of street trees affects the performance in simulating surface energy fluxes is further analyzed. Fig. 6 shows the mean diurnal variations of net radiation, sensible heat flux, and latent heat flux ensemble-averaged over the SNUUCM-Tree simulations with the 274 Pareto-optimal parameter sets in the Tree-on case and those with the 346 Pareto-optimal parameter sets in the Tree-off case during the analysis period and their scatterplots against observations. Here, to perform an in-depth analysis of the effects of including street trees on the simulation errors of surface energy fluxes, the systematic and unsystematic RMSEs (hereafter, $RMSE_s$ and $RMSE_u$, respectively) for the three energy fluxes in the Tree-on and Tree-off cases are calculated (Willmott, 1981) and compared with each other.

In the Tree-off case, the systematic underestimation of net radiation is found in the daytime (Fig. 6a and c), its $RMSE_s$ being 21.3 W m^{-2} and $RMSE_u$ being 22.6 W m^{-2}. Compared with the Tree-off case, in the Tree-on case, the systematic biases in net radiation become much smaller both in the daytime and nighttime, its $RMSE_s$ being only 1.9 W m^{-2} and $RMSE_u$ being 7.9 W m^{-2} (Fig. 6a and b). The sensible heat flux is systematically overestimated, particularly in the daytime in the Tree-off case with its $RMSE_s$ of 18.9 W m^{-2}

(Fig. 6d and f). The considerable unsystematic errors in sensible heat flux are also found in the Tree-off case, its $\mathrm{RMSE_u}$ reaching 50.4 W m^{-2}. The inclusion of street trees reduces both systematic and unsystematic errors in sensible heat flux, with its $\mathrm{RMSE_s}$ of 8.9 W m^{-2} and $\mathrm{RMSE_u}$ of 35.6 W m^{-2} in the Tree-on case (Fig. 6e). The reduction in systematic errors resulting from the inclusion of street trees is more evident in the daytime than in the nighttime, and a slight systematic underestimation of sensible heat flux in the daytime is seen in the Tree-on case. In the Tree-off case, the latent heat flux is considerably underestimated throughout the day, its $\mathrm{RMSE_s}$ and $\mathrm{RMSE_u}$ being 44.3 W m^{-2} and 40.0 W m^{-2}, respectively (Fig. 6g and i). The inclusion of street trees enables a satisfactory reproduction of the diurnal variation of latent heat flux, considerably reducing the systematic low biases (Fig. 6g and h). $\mathrm{RMSE_s}$ for latent heat flux in the Tree-on case is 12.8 W m^{-2} and is much smaller than $\mathrm{RMSE_u}$ for latent heat flux (26.7 W m^{-2}), in contrast to the Tree-off case in which $\mathrm{RMSE_s}$ exceeds $\mathrm{RMSE_u}$ for latent heat flux.

The above results show that the inclusion of street trees can lead to notable reductions in systematic errors in simulated surface energy fluxes as well as in their unsystematic errors. The reductions in systematic errors in simulated surface energy fluxes due to the inclusion of street trees were also found in several previous studies (e.g., Liu et al., 2017; Mussetti et al., 2020). The improvements in overall performances and substantial reductions in $\mathrm{RMSE_s}$ for the three energy fluxes are also found at the Basel-Spalrenring site (Figs. S2 and S3). However, at this site, the inclusion of street trees slightly enhances the overestimation of sensible heat flux and the underestimation of latent heat flux in the daytime is still pronounced in the Tree-on case. This implies the necessities of further improvements in the partitioning between sensible and latent heat fluxes and/or in the specification of other parameters associated with evapotranspiration for this vegetated urban site.

The trade-off between the performance in simulating net radiation and that in simulating sensible heat flux is a well-known issue in earlier UCMs without representing street trees (Chen et al., 2011; Grimmond et al., 2011). How the inclusion of street trees affects this trade-off is examined in Fig. 7. Fig. 7 shows the scatterplots of $RMSE_{RN}$ versus $RMSE_{SH}$ within the Pareto-optimal sets in the Tree-on and Tree-off cases with $RMSE_{LH}$ being colored. In the Tree-off case, the clear negative correlation between $RMSE_{RN}$ and $RMSE_{SH}$ is found (Fig. 7b) with a correlation coefficient (R) of −0.60 ($p < 0.001$), which means that improving the simulation of net radiation tends to degrade that of sensible heat flux and vice versa. This is indicative of the existence of the trade-off between the performances in simulating net radiation and sensible heat flux, as identified in UCMs without representing street trees (Loridan et al., 2010; Demuzere et al., 2017). Within the Pareto-optimal sets, $RMSE_{SH}$ can be further reduced by up to 30.6 W m^{-2} while this is accompanied by an increase in $RMSE_{RN}$ by 45.7 W m^{-2}. The negative correlation is also found between $RMSE_{RN}$ and $RMSE_{LH}$, but the trade-off between the performances in simulating net radiation and latent heat flux is very weak. In the Tree-on case, although there is still negative correlation between $RMSE_{RN}$ and $RMSE_{SH}$ (Fig. 7a) with R of −0.32 ($p < 0.001$), the trade-off between the simulation performances of net radiation and sensible heat flux becomes weaker with the regression slope of $RMSE_{SH}$ with respect to $RMSE_{RN}$ being smaller by 39% compared to that in the Tree-off case. The weakening of this trade-off due to the inclusion of street trees is also found at the Basel-Spalrenring site (Fig. S4). In addition, there is a positive correlation between $RMSE_{SH}$ and $RMSE_{LH}$ in the Tree-on case (Fig. 7a) with R of 0.61 ($p < 0.001$), which indicates that the simultaneous improvements in the simulations of sensible and latent heat fluxes can be achieved in the presence of street trees.

Through the results of Figs. 4–7, it is revealed that the inclusion of street trees can reduce the trade-offs among surface energy fluxes and thus substantially enhance the maximum achievable accuracy of urban surface energy flux simulations. To further understand the model behavior and gain insights into the prioritization of parameter calibrations, it is crucial to identify relatively sensitive input parameters (Voudouri et al., 2017). In the following subsection, how the tree-related parameters are important for simulating surface energy fluxes relative to the urban thermal parameters is examined by ranking the sensitivities to individual parameters through the Sobol' method.

3.2. Model sensitivities to tree-related parameters

Fig. 8 shows the bar charts of the total-order Sobol' indices of the tree-related parameters and urban thermal parameters for $RMSE_{RN}$, $RMSE_{SH}$, and $RMSE_{LH}$ at the Basel-Sperrstrasse site. For $RMSE_{RN}$, α_r exhibits by far the largest total-order Sobol' index (0.84) among all the parameters (Fig. 8a). For the sensitivity of $RMSE_{RN}$ to α_r, the first-order effect dominates over the interaction effect, indicating that α_r alone has a crucial influence on the simulation of net radiation and thus its proper specification can lead to a substantial improvement in the simulation performance of net radiation. The second largest total-order Sobol' index appears for f_t (0.10) but is much smaller than that of α_r. The strong sensitivity of simulated net radiation to α_r and very weak sensitivities to road-related thermal parameters are consistent with the results from other UCMs without representing street trees (Loridan et al., 2010; Ao and Zhang, 2022).

For $RMSE_{SH}$, the largest total-order Sobol' index appears also for α_r (0.40) and the second largest total-order Sobol' index appears for C_r (0.30) (Fig. 8b). Previous studies employing UCMs without representing street trees have also reported the strong influence of roof-related parameters on simulating sensible heat flux as well as net radiation (e.g., Zhao et al., 2014; Ao and Zhang, 2022). Unlike for $RMSE_{RN}$, the interaction effect is comparably or more important compared with the first-order effect for the sensitivities of $RMSE_{SH}$ to the major influential parameters. This indicates that the simultaneous optimization of multiple parameters is needed to effectively improve the simulation performance of sensible heat flux. f_t exhibits the third largest total-order Sobol' index (0.19), with its interaction effect (0.16) far exceeding its first-order effect (0.03). Interestingly, the second-order Sobol' index is the largest between α_r and f_t, being 0.08 (not shown). This suggests that the simultaneous optimization of these two parameters can synergistically reduce $RMSE_{SH}$.

For $RMSE_{LH}$, the two tree-related parameters, f_t and a_t, exhibit the largest total-order Sobol' indices (0.89 and 0.38, respectively) (Fig. 8c), indicating that they are the most influential parameters for the simulation of latent heat flux. This is possibly due to that the evapotranspiration from street trees is the primary source of latent heat flux. The third largest total-order Sobol' index appears for α_w (0.14), and given that the second-order Sobol indices with f_t and a_t (0.07 and 0.02, respectively) largely account for it (not shown), the accurate simulation of shortwave radiation reflections from walls to street trees appears to be also important in improving the simulation of latent heat flux. It is also found that the interaction effect between f_t and a_t is comparable or more important compared with their first-order effects for the sensitivities of $RMSE_{LH}$ to f_t and a_t. Thus, to reduce $RMSE_{LH}$, the appropriate specification of both f_t and a_t is of foremost importance.

How the relative importance of the tree-related and urban thermal parameters differs in the simulations of net radiation, sensible heat flux, and latent heat flux at a vegetated urban site is analyzed. Fig. 9 is the same as Fig. 8 except for the Basel-Spalrenring site. Unlike at the Basel-Sperrstrasse site, the tree-related parameters have the strongest influence on all

$RMSE_{RN}$, $RMSE_{SH}$, and $RMSE_{LH}$ (Fig. 9): a_t exhibits the largest total-order Sobol' index for $RMSE_{RN}$ (Fig. 9a), and f_t and a_t, respectively, exhibit the first and second largest total-order Sobol' indices for both $RMSE_{SH}$ and $RMSE_{LH}$ (Fig. 9b and c). α_r, the most influential parameter for both $RMSE_{RN}$ and $RMSE_{SH}$ at the Basel-Sperrstrasse site, has comparable influence to f_t for $RMSE_{RN}$ and to a_t for $RMSE_{SH}$ at this site. These results reveal that the appropriate specification of the tree-related parameters is much more important for improving the simulation performances of the three energy fluxes than that of the urban thermal parameters at this vegetated urban site. Compared with the Basel-Sperrstrasse site, at the Basel-Spalrenring site, the interaction effects among the parameters are more important for the sensitivity of $RMSE_{RN}$ while they are less important for the sensitivities of $RMSE_{SH}$ and $RMSE_{LH}$. This suggests that the relationships between the input parameters and simulation performance of net radiation (turbulent heat fluxes) are more (less) complex at the vegetated urban site than at the dense urban site.

4. Summary and conclusions

This study examines the effects of including street trees on the performances in simulating surface energy fluxes and compares their sensitivities to tree-related parameters with their sensitivities to urban thermal parameters using the Sobol' method. The street trees and their related physical processes are newly represented in the SNUUCM (SNUUCM-Tree), and the multi-objective parameter optimization is conducted for the Tree-on and Tree-off cases to robustly evaluate how much the inclusion of street trees can improve the simulation performances of surface energy fluxes. To efficiently conduct both parameter optimization and sensitivity analysis, the ML models to predict the UCM performances from the given input parameters are constructed. The RMSEs of all net radiation, sensible heat flux, and latent heat flux are notably lower in the Tree-on case than in the Tree-off case, revealing that the inclusion of street trees significantly raises the maximum achievable performances in simulating surface energy fluxes. In addition, the inclusion of street trees reduces the trade-off between the performance in simulating net radiation and that in simulating sensible heat flux, allowing more effective improvements in the simulations of the three energy fluxes through parameter optimization. At the dense urban (Basel-Sperrstrasse) site, the sensitivities of the RMSEs of net radiation and sensible heat flux are the largest for roof albedo and that of latent heat flux is the largest for tree fraction. Meanwhile, at the vegetated urban (Basel-Spalrenring) site, the largest sensitivities of the RMSEs of all the three energy fluxes appear for the tree-related parameters.

In this study, an ML-based framework that enables parameter optimization and sensitivity analysis to be very efficiently performed by replacing numerous UCM simulations is presented. In such a way, the ML-based approach can be utilized in various aspects of urban weather/climate modeling studies with much less computational costs compared with the sole use of physics-based models (e.g., Lange et al., 2021; Wu et al., 2021). Future applications of an extended ML-based framework, such as surrogate modeling of UCM-simulated surface energy fluxes and canyon air temperature, are expected to further enhance the understanding of UCM behaviors and be helpful for the studies of urban heat and its mitigation.

In addition to the input parameters selected in this study, various other input parameters can also significantly affect the simulations of urban surface energy fluxes. For example, soil moisture is an important factor affecting tree evapotranspiration (Lagergren and Lindroth, 2002) and the effects of street trees on urban surface energy fluxes can largely differ depending on urban morphological characteristics (Ryu et al., 2025). Further investigations considering a broader range of input parameters would provide more valuable insights into the effects of street trees on the simulations of urban surface energy fluxes.

The analyses in this study are conducted for the two adjacent urban sites with different surroundings under the same background climate. It was found that the sensitivities of urban surface energy fluxes to tree-related parameters can significantly vary depending on background climates (Meili et al., 2020). An extensive investigation for various urban sites with different background climates is needed for better understanding of the relationships between tree-related parameters and surface energy fluxes.

CRediT authorship contribution statement

Kyeongjoo Park: Writing – Review & Editing, Writing – Original Draft, Methodology, Software, Validation, Formal analysis, Investigation, Data curation, Visualization. **Jong-Jin Baik:** Writing – Review & Editing, Supervision, Methodology, Formal analysis, Conceptualization. **Young-Hee Ryu:** Writing – Review & Editing, Methodology, Software, Investigation.

Declaration of competing interest

The authors declare that they have no known competing financial interests or personal relationships that could have appeared to influence the work reported in this paper.

Acknowledgements

This work was supported by the National Research Foundation of Korea (NRF) under grant RS-2025-00562044. The authors acknowledge the use of the BUBBLE campaign dataset that was funded by the Swiss Ministry of Education and Science (grant C00.0068) and the University of Basel, the Swiss Federal Institute of Technology (ETH) Zürich, the Technical University of Dresden, and the Bulgarian National Institute of Meteorology and Hydrology.

References

Akiba, T., Sano, S., Yanase, T., Ohta, T., Koyama, M., 2019. Optuna: a next-generation hyperparameter optimization framework. In: Proceedings of the 25th ACM SIGKDD International Conference on Knowledge Discovery and Data Mining, pp. 2623–2631.

Ao, X., Zhang, N., 2022. Parameter sensitivity analysis and optimization of the single-layer urban canopy model in the megacity of Shanghai. Adv. Meteorol. 2022, 7351150.

Başağaoğlu, H., Chakraborty, D., Do Lago, C., Gutierrez, L., Şahinli, M.A., Giacomoni, M., Furl, C., Mirchi, A., Moriasi, D., Şengör, S.S., 2022. A review on interpretable and explainable artificial intelligence in hydroclimatic applications. Water 14, 1230.

Chen, F., Dudhia, J., 2001. Coupling an advanced land surface–hydrology model with the Penn State–NCAR MM5 modeling system. Part I: model implementation and sensitivity. Mon. Weather Rev. 129, 569–585.

Chen, F., Kusaka, H., Bornstein, R., Ching, J., Grimmond, C.S.B., Grossman-Clarke, S., Loridan, T., Manning, K.W., Martilli, A., Miao, S., Sailor, D., Salamanca, F.P., Taha, H., Tewari, M., Wang, X., Wyszogrodzki, A.A., Zhang, C., 2011. The integrated

WRF/urban modelling system: development, evaluation, and applications to urban environmental problems. Int. J. Climatol. 31, 273–288.

Chen, T., Guestrin, C., 2016. XGBoost: a scalable tree boosting system. In: Proceedings of the 22nd ACM SIGKDD International Conference on Knowledge Discovery and Data Mining, pp. 785–794.

Ching, J.K.S., 2013. A perspective on urban canopy layer modeling for weather, climate and air quality applications. Urban Clim. 3, 13–39.

Christen, A., Vogt, R., 2004. Energy and radiation balance of a central European city. Int. J. Climatol. 24, 1395–1421.

Deb, K., Jain, H., 2013. An evolutionary many-objective optimization algorithm using reference-point-based nondominated sorting approach, part I: solving problems with box constraints. IEEE Trans. Evol. Comput. 18, 577–601.

Demuzere, M., Harshan, S., Järvi, L., Roth, M., Grimmond, C.S.B., Masson, V., Oleson, K.W., Velasco, E., Wouters, H., 2017. Impact of urban canopy models and external parameters on the modelled urban energy balance in a tropical city. Q. J. R. Meteorol. Soc. 143, 1581–1596.

Green, S.R., 1993. Radiation balance, transpiration and photosynthesis of an isolated tree. Agric. For. Meteorol. 64, 201–221.

Grimmond, C.S.B., Blackett, M., Best, M.J., Baik, J.-J., Belcher, S.E., Beringer, J., Bohnenstengel, S.I., Calmet, I., Chen, F., Coutts, A., Dandou, A., Fortuniak, K., Gouvea, M.L., Hamdi, R., Hendry, M., Kanda, M., Kawai, T., Kawamoto, Y., Kondo, H., Krayenhoff, E.S., Lee, S.-H., Loridan, T., Martilli, A., Masson, V., Miao, S., Oleson, K., Ooka, R., Pigeon, G., Porson, A., Ryu, Y.-H., Salamanca, F., Steeneveld, G.J., Tombrou, M., Voogt, J.A., Young, D.T., Zhang, N., 2011. Initial results from

Phase 2 of the international urban energy balance model comparison. Int. J. Climatol. 31, 244–272.

Grimmond, C.S.B., Blackett, M., Best, M.J., Barlow, J., Baik, J.-J., Belcher, S.E., Bohnenstengel, S.I., Calmet, I., Chen, F., Dandou, A., Fortuniak, K., Gouvea, M.L., Hamdi, R., Hendry, M., Kawai, T., Kawamoto, Y., Kondo, H., Krayenhoff, E.S., Lee, S.-H., Loridan, T., Martilli, A., Masson, V., Miao, S., Oleson, K., Pigeon, G., Porson, A., Ryu, Y.-H., Salamanca, F., Shashua-Bar, L., Steeneveld, G.-J., Tombrou, M., Voogt, J., Young, D., Zhang, N., 2010. The international urban energy balance models comparison project: first results from phase 1. J. Appl. Meteorol. Climatol. 49, 1268–1292.

Hamdi, R., Kusaka, H., Doan, Q.-V., Cai, P., He, H., Luo, G., Kuang, W., Caluwaerts, S., Duchêne, F., Van Schaeybroek, B., Termonia, P., 2020. The state-of-the-art of urban climate change modeling and observations. Earth Syst. Environ. 4, 631–646.

Hanberry, B.B., 2023. Urban land expansion and decreased urban sprawl at global, national, and city scales during 2000 to 2020. Ecosyst. Health Sustain. 9, 0074.

Hora, G.S., Giometto, M.G., 2024. Surrogate modeling of urban boundary layer flows. Phys. Fluids 36, 076625.

Hu, C., Tam, C.-Y., Yang, Z.-l., Wang, Z., 2024. Analyzing urban influence on extreme winter precipitation through observations and numerical simulation of two South China case studies. Sci. Rep. 14, 2099.

Jandaghian, Z., Berardi, U., 2020. Comparing urban canopy models for microclimate simulations in Weather Research and Forecasting Models. Sust. Cities Soc. 55, 102025.

Jongen, H.J., Lipson, M., Teuling, A.J., Grimmond, S., Baik, J.-J., Best, M., Demuzere, M., Fortuniak, K., Huang, Y., De Kauwe, M.G., Li, R., McNorton, J., Meili, N., Oleson, K., Park, S.-B., Sun, T., Tsiringakis, A., Varentsov, M., Wang, C., Wang, Z.-H., Steeneveld, G.J., 2024. The water balance representation in Urban-PLUMBER land surface models. J. Adv. Model. Earth Syst. 16, e2024MS004231.

Katoch, S., Chauhan, S.S., Kumar, V., 2021. A review on genetic algorithm: past, present, and future. Multimed. Tools Appl. 80, 8091–8126.

Krayenhoff, E.S., Christen, A., Martilli, A., Oke, T.R., 2014. A multi-layer radiation model for urban neighbourhoods with trees. Bound.-Layer Meteorol. 151, 139–178.

Krayenhoff, E.S., Jiang, T., Christen, A., Martilli, A., Oke, T.R., Bailey, B.N., Nazarian, N., Voogt, J.A., Giometto, M.G., Stastny, A., Crawford, B.R., 2020. A multi-layer urban canopy meteorological model with trees (BEP-Tree): street tree impacts on pedestrian-level climate. Urban Clim. 32, 100590.

Kusaka, H., Chen, F., Tewari, M., Dudhia, J., Gill, D.O., Duda, M.G., Wang, W., Miya, Y., 2012. Numerical simulation of urban heat island effect by the WRF model with 4-km grid increment: an inter-comparison study between the urban canopy model and slab model. J. Meteorol. Soc. Jpn. 90B, 33–45.

Kusaka, H., Kondo, H., Kikegawa, Y., Kimura, F., 2001. A simple single-layer urban canopy model for atmospheric models: comparison with multi-layer and slab models. Bound.-Layer Meteorol. 101, 329–358.

Lagergren, F., Lindroth, A., 2002. Transpiration response to soil moisture in pine and spruce trees in Sweden. Agric. For. Meteorol. 112, 67–85.

Landsberg, J.J., Powell, D.B.B., 1973. Surface exchange characteristics of leaves subject to mutual interference. Agric. Meteorol. 12, 169–184.

Lange, M., Suominen, H., Kurppa, M., Järvi, L., Oikarinen, E., Savvides, R., Puolamäki, K.,

2021. Machine-learning models to replicate large-eddy simulations of air pollutant concentrations along boulevard-type streets. Geosci. Model Dev. 14, 7411–7424.

Li, P., Xu, T., Wei, S., Wang, Z.-H., 2022. Multi-objective optimization of urban environmental system design using machine learning. Comput. Environ. Urban Syst. 94, 101796.

Lipson, M.J., Grimmond, S., Best, M., Abramowitz, G., Coutts, A., Tapper, N., Baik, J.-J., Beyers, M., Blunn, L., Boussetta, S., Bou-Zeid, E., De Kauwe, M.G., de Munck, C., Demuzere, M., Fatichi, S., Fortuniak, K., Han, B.-S., Hendry, M.A., Kikegawa, Y., Kondo, H., Lee, D.-I., Lee, S.-H., Lemonsu, A., Machado, T., Manoli, G., Martilli, A., Masson, V., McNorton, J., Meili, N., Meyer, D., Nice, K.A., Oleson, K.W., Park, S.-B., Roth, M., Schoetter, R., Simón-Moral, A., Steeneveld, G.-J., Sun, T., Takane, Y., Thatcher, M., Tsiringakis, A., Varentsov, M., Wang, C., Wang, Z.-H., Pitman, A.J., 2024. Evaluation of 30 urban land surface models in the Urban-PLUMBER project: phase 1 results. Q. J. R. Meteorol. Soc. 150, 126–169.

Liu, X., Li, X.-X., Harshan, S., Roth, M., Velasco, E., 2017. Evaluation of an urban canopy model in a tropical city: the role of tree evapotranspiration. Environ. Res. Lett. 12, 094008.

Loridan, T., Grimmond, C.S.B., Grossman-Clarke, S., Chen, F., Tewari, M., Manning, K., Martilli, A., Kusaka, H., Best, M., 2010. Trade-offs and responsiveness of the single-layer urban canopy parametrization in WRF: an offline evaluation using the MOSCEM optimization algorithm and field observations. Q. J. R. Meteorol. Soc. 136, 997–1019.

Lu, Y., Zhou, X.-H., Xiao, H., Li, Q., 2022. Using machine learning to predict urban canopy flows for land surface modeling. Geophys. Res. Lett. 50, e2022GL102313.

Martilli, A., Clappier, A., Rotach, M.W., 2002. An urban surface exchange parameterisation for mesoscale models. Bound.-Layer Meteorol. 104, 261–304.

Masson, V., 2000. A physically-based scheme for the urban energy budget in atmospheric models. Bound.-Layer Meteorol. 94, 357–397.

McKay, M.D., Beckman, R.J., Conover, W.J., 1979. A comparison of three methods for selecting values of input variables in the analysis of output from a computer code. Technometrics 21, 239–245.

Meili, N., Manoli, G., Burlando, P., Bou-Zeid, E., Chow, W.T.L., Coutts, A.M., Daly, E., Nice, K.A., Roth, M., Tapper, N.J., Velasco, E., Vivoni, E.R., Fatichi, S., 2020. An urban ecohydrological model to quantify the effect of vegetation on urban climate and hydrology (UT&C v1.0). Geosci. Model Dev. 13, 335–362.

Meili, N., Manoli, G., Burlando, P., Carmeliet, J., Chow, W.T.L., Coutts, A.M., Roth, M., Velasco, E., Vivoni, E.R., Fatichi, S., 2021. Tree effects on urban microclimate: diurnal, seasonal, and climatic temperature differences explained by separating radiation, evapotranspiration, and roughness effects. Urban For. Urban Green. 58, 126970.

Mussetti, G., Brunner, D., Henne, S., Allegrini, J., Krayenhoff, E.S., Schubert, S., Feigenwinter, C., Vogt, R., Wicki, A., Carmeliet, J., 2020. COSMO-BEP-Tree v1.0: a coupled urban climate model with explicit representation of street trees. Geosci. Model Dev. 13, 1685–1710.

Nemunaitis-Berry, K.L., Klein, P.M., Basara, J.B., Fedorovich, E., 2017. Sensitivity of predictions of the urban surface energy balance and heat island to variations of urban canopy parameters in simulations with the WRF model. J. Appl. Meteorol. Climatol. 56, 573–595.

Oleson, K.W., Bonan, G.B., Feddema, J., Vertenstein, M., Grimmond, C.S.B., 2008. An urban parameterization for a global climate model. Part I: formulation and evaluation for two cities. J. Appl. Meteorol. Climatol. 47, 1038–1060.

Qian, Y., Chakraborty, T.C., Li, J., Li, D., He, C., Sarangi, C., Chen, F., Yang, X., Leung, L.R., 2022. Urbanization impact on regional climate and extreme weather: current understanding, uncertainties, and future research directions. Adv. Atmos. Sci. 39, 819–860.

Rotach, M.W., Vogt, R., Bernhofer, C., Batchvarova, E., Christen, A., Clappier, A., Feddersen, B., Gryning, S.-E., Martucci, G., Mayer, H., Mitev, V., Oke, T.R., Parlow, E., Richner, H., Roth, M., Roulet, Y.-A., Ruffieux, D., Salmond, J.A., Schatzmann, M., Voogt, J.A., 2005. BUBBLE – an urban boundary layer meteorology project. Theor. Appl. Climatol. 81, 231–261.

Ryu, Y.-H., Baik, J.-J., Lee, S.-H., 2011. A new single-layer urban canopy model for use in mesoscale atmospheric models. J. Appl. Meteorol. Climatol. 50, 1773–1794.

Ryu, Y.-H., Bou-Zeid, E., Wang, Z.-H., Smith, J.A., 2016. Realistic representation of trees in an urban canopy model. Bound.-Layer Meteorol. 159, 193–220.

Ryu, Y.-H., Kim, S., Park, M.-S., Lee, J., Kim, J., Kang, M., 2025. Online coupling of an urban canopy model with trees and a mesoscale atmospheric model to assess the cooling effects of trees under different urban configurations and varying soil dryness. Sust. Cities Soc. 121, 106226.

Seto, K.C., Fragkias, M., Güneralp, B., Reilly, M.K., 2011. A meta-analysis of global urban land expansion. PLoS One 6, e23777.

Shao, L., Liao, W., Li, P., Luo, M., Xiong, X., Liu, X., 2023. Drivers of global surface urban heat islands: surface property, climate background, and 2D/3D urban morphologies.

Build. Environ. 242, 110581.

Sharma, S., Kumar, V., 2022. A comprehensive review on multi-objective optimization techniques: past, present and future. Arch. Comput. Method Eng. 29, 5605–5633.

Sobol’, I.M., 1967. On the distribution of points in a cube and the approximate evaluation of integrals. USSR Comput. Math. Math. Phys. 7, 86–112.

Sobolʹ, I.M., 2001. Global sensitivity indices for nonlinear mathematical models and their Monte Carlo estimates. Math. Comput. Simul. 55, 271–280.

Song, X., Zhang, J., Zhan, C., Xuan, Y., Ye, M., Xu, C., 2015. Global sensitivity analysis in hydrological modeling: review of concepts, methods, theoretical framework, and applications. J. Hydrol. 523, 739–757.

Tanoori, G., Soltani, A., Modiri, A., 2024. Machine learning for urban heat island (UHI) analysis: predicting land surface temperature (LST) in urban environments. Urban Clim. 55, 101962.

Tian, W., 2013. A review of sensitivity analysis methods in building energy analysis. Renew. Sust. Energ. Rev. 20, 411–419.

Tsiringakis, A., Holtslag, A.A.M., Grimmond, S., Steeneveld, G.J., 2020. Surface and atmospheric driven variability of the single-layer urban canopy model under clear-sky conditions over London. J. Geophys. Res. Atmos. 125, e2019JD032167.

Tsiringakis, A., Steeneveld, G.-J., Holtslag, A.A.M., Kotthaus, S., Grimmond, S., 2019. On- and off-line evaluation of the single-layer urban canopy model in London summertime conditions. Q. J. R. Meteorol. Soc. 145, 1474–1489.

Van Stein, B., Raponi, E., Sadeghi, Z., Bouman, N., Van Ham, R.C.H.J., Bäck, T., 2022. A comparison of global sensitivity analysis methods for explainable AI with an application in genomic prediction. IEEE Access 10, 103364–103381.

Voudouri, A., Khain, P., Carmona, I., Bellprat, O., Grazzini, F., Avgoustoglou, E., Bettems, J.M, Kaufmann P., 2017. Objective calibration of numerical weather prediction models. Atmos. Res. 190, 128–140.

Wang, C., Wang, Z.-H., Ryu, Y.-H., 2021. A single-layer urban canopy model with transmissive radiation exchange between trees and street canyons. Build. Environ. 191, 107593.

Wang, Z.-H., 2014. Monte Carlo simulations of radiative heat exchange in a street canyon with trees. Sol. Energy 110, 704–713.

Wang, Z.-H., Bou-Zeid, E., Au, S.K., Smith, J.A., 2011. Analyzing the sensitivity of WRF's single-layer urban canopy model to parameter uncertainty using advanced Monte Carlo simulation. J. Appl. Meteorol. Climatol. 50, 1795–1814.

Wang, Z.-H., Bou-Zeid, E., Smith, J.A., 2013. A coupled energy transport and hydrological model for urban canopies evaluated using a wireless sensor network. Q. J. R. Meteorol. Soc. 139, 1643–1657.

Werth, D., Buckley, R., 2022. The application of a genetic algorithm to the optimization of a mesoscale model for emergency response. J. Appl. Meteorol. Climatol. 61, 329–343.

Willmott, C.J., 1981. On the validation of models. Phys. Geogr. 2, 184–194.

Wu, Y., Teufel, B., Sushama, L., Belair, S., Sun, L., 2021. Deep learning-based super-resolution climate simulator-emulator framework for urban heat studies. Geophys. Res. Lett. 48, e2021GL094737.

Yang, J., Wang, Z.-H., 2014. Physical parameterization and sensitivity of urban hydrological models: application to green roof systems. Build. Environ. 75, 250–263.

Zhang, Y., Teoh, B.K., Zhang, L., 2024. Multi-objective optimization for energy-efficient building design considering urban heat island effects. Appl. Energy 376, 124117.

Zhao, W., Zhang, N., Sun, J., Zou, J., 2014. Evaluation and parameter-sensitivity study of a single-layer urban canopy model (SLUCM) with measurements in Nanjing, China. J. Hydrometeorol. 15, 1078–1090.

Zhao, Y., Jiang, C., Vega, M.A., Todd, M.D., Hu, Z., 2023. Surrogate modeling of nonlinear dynamic systems: a comparative study. J. Comput. Inf. Sci. Eng. 23, 011001.

Zhao, Z., Li, H., Wang, S., 2024. Machine learning-based surrogate models for fast impact assessment of a new building on urban local microclimate at design stage. Build. Environ. 266, 112142.

Zhou, H., Gao, C., Luan, Q., Shi, L., Lu, Z., and Liu, J., 2024a. Multi-objective optimization of distributed green infrastructure for effective stormwater management in space-constrained highly urbanized areas. J. Hydrol. 644, 132065.

Zhou, W., Zhang, L., Wang, G., Zhang, Q., Cao, H., Zhang, H., Jia, B., Tang, Z., Li, X., Liu, L., 2024b. Impacts of urban expansion on air temperature and humidity during 2022 mega-heatwave over the Yangtze River Delta, China. Sci. Total Environ. 951, 175804.

Table 1

Formulations of key physical processes newly added or modified in the SNUUCM-Tree.

Equations	Descriptions of symbols
View factors	
$F_{\mathrm{gs}} = -0.2462 \times \frac{H}{W} - 1.1568 \times \frac{a_{\mathrm{t}}}{W} + 0.7217$ (1) $F_{\mathrm{gt}} = -0.0024 \times \frac{H}{W} - 1.9822 \times \frac{a_{\mathrm{t}}}{W} - 0.0078$ (2) $F_{\mathrm{gw}} = 0.5 \times (1 - F_{\mathrm{gs}} - F_{\mathrm{gt}})$ (3) $F_{\mathrm{ww}} = 0.3069 \times \frac{H}{W} - 1.1938 \times \frac{a_{\mathrm{t}}}{W} + 0.0999$ (4) $F_{\mathrm{wt}} = -0.2655 \times \frac{H}{W} + 2.7254 \times \frac{a_{\mathrm{t}}}{W} + 0.2863$ (5) $F_{\mathrm{ws}} = 0.5 \times (1 - F_{\mathrm{ww}} - F_{\mathrm{wt}})$ (6) $F_{\mathrm{wg}} = 0.5 \times (1 - F_{\mathrm{ww}} - F_{\mathrm{wt}})$ (7) $F_{\mathrm{ts}} = -0.2018 \times \frac{H}{W} + 0.2158 \times \frac{a_{\mathrm{t}}}{W} + 0.4871$ (8) $F_{\mathrm{tw}} = 0.5 \times \left(0.1210 \times \frac{H}{W} - 0.0242 \times \frac{a_{\mathrm{t}}}{W} + 0.2368 \right)$ (9) $F_{\mathrm{tt}} = -0.0716 \times \frac{H}{W} + 0.4082 \times \frac{a_{\mathrm{t}}}{W} + 0.1563$ (10) $F_{\mathrm{tg}} = 1 - F_{\mathrm{ts}} - 2 \times F_{\mathrm{tw}} - F_{\mathrm{tt}}$ (11)	F_{12}: view factors from surface 1 to surface 2 g: ground s: sky t: tree w: wall H: building height W: canyon width a_{t}: tree-crown radius
Radiation	
$S_{i,\,\mathrm{wtree}}^{\mathrm{net}} = (1-\alpha_i) S_i^{\mathrm{in}} + (1-\alpha_i) \sum_j S_j^{\mathrm{in}} \alpha_j \frac{A_j}{A_i} F_{ji} + (1-\alpha_i) \sum_j \sum_k S_j^{\mathrm{in}} \alpha_j \frac{A_j}{A_k} F_{jk} \alpha_k \frac{A_k}{A_i} F_{ki} + \sum_j \sum_k \sum_l S_j^{\mathrm{in}} \alpha_j \frac{A_j}{A_k} F_{jk} \alpha_k \frac{A_k}{A_l} F_{kl} \alpha_l \frac{A_l}{A_i} F_{li}$ (12) $L_{i,\,\mathrm{wtree}}^{\mathrm{net}} = \varepsilon_i \sum_j L_j \frac{A_j}{A_i} F_{ji} + \sum_j \sum_k L_j \frac{A_j}{A_k} F_{jk} (1-\varepsilon_k) \frac{A_k}{A_i} F_{ki} - \varepsilon_i \sigma T_i^4$ (13) $\overline{S_i^{\mathrm{net}}} = f_{\mathrm{t}} S_{i,\mathrm{wtree}}^{\mathrm{net}} + (1 - f_{\mathrm{t}}) S_{i,\mathrm{wotree}}^{\mathrm{net}}$ (14) $\overline{L_i^{\mathrm{net}}} = f_{\mathrm{t}} L_{i,\mathrm{wtree}}^{\mathrm{net}} + (1 - f_{\mathrm{t}}) L_{i,\mathrm{wotree}}^{\mathrm{net}}$ (15)	S^{net} (S^{in}): net (incident) shortwave radiation L^{net} (L): net (emitted) longwave radiation wtree (wotree): with (without) street trees i: index indicating in-canyon surfaces j, k, l: indices indicating in-canyon surfaces (or sky in Eq. (13)) α (ε): albedo (emissivity) A: area $\overline{}$: weighted average f_{t}: tree fraction

Table 2

Formulations of key physical processes newly added or modified in the SNUUCM-Tree (continued).

	Equations	Descriptions of symbols
Leaf turbulent heat fluxes		
	$$Q_{\mathrm{H,l}} = \frac{\rho c_{\mathrm{p}} (T_{\mathrm{l}} - T_{\mathrm{c}})}{1.27 r_a} \quad (16)$$ $$Q_{\mathrm{E,l}} = \frac{s Q_{\mathrm{l}}^{*} + 0.93 \rho c_{\mathrm{p}} \frac{D_{\mathrm{a}}}{r_{\mathrm{a}}}}{s + 0.93\gamma (2 + \frac{r_{\mathrm{s}}}{r_{\mathrm{a}}})} \quad (17)$$	Q_{H}: sensible heat flux Q_{E}: latent heat flux l: leaf ρ: air density c_{p}: specific heat of dry air at constant pressure T: temperature c: canyon air r_{a}: aerodynamic resistance s: slope of the saturation vapor pressure curve at ambient temperature Q^{*}: net radiation D_{a}: vapor pressure deficit γ: psychometric constant r_{s}: surface resistance
Temperature and humidity		
	$$\rho c_{\mathrm{p}} V_c \frac{dT_c}{dt} = \left(\frac{H}{W} Q_{\mathrm{H,w1}} + \frac{H}{W} Q_{\mathrm{H,w2}} + f_{\mathrm{vg}} Q_{\mathrm{H,vg}} + (1 - f_{\mathrm{vg}}) Q_{\mathrm{H,ig}} + 2 f_{\mathrm{t}} \frac{A_{\mathrm{l}}}{W} Q_{\mathrm{H,l}} + Q_{\mathrm{AH}} - Q_{\mathrm{H,c}} \right) A_{\mathrm{c}} \quad (18)$$ $$\rho c_{\mathrm{p}} V_c \frac{dq_c}{dt} = \left(\frac{H}{W} Q_{\mathrm{E,w1}} + \frac{H}{W} Q_{\mathrm{E,w2}} + f_{\mathrm{vg}} Q_{\mathrm{E,vg}} + (1 - f_{\mathrm{vg}}) Q_{\mathrm{E,ig}} + 2 f_{\mathrm{t}} \frac{A_{\mathrm{l}}}{W} Q_{\mathrm{E,l}} - Q_{\mathrm{E,c}} \right) A_{\mathrm{c}} \quad (19)$$ $$C_{\mathrm{l}} \frac{dT_{\mathrm{l}}}{dt} = \left(Q_{\mathrm{l}}^{*} - Q_{\mathrm{H,l}} - Q_{\mathrm{E,l}} \right) \quad (20)$$	V_{c}: canyon air volume q: specific humidity C_{l}: leaf heat capacity w1: wall 1 w2: wall 2 vg: vegetated ground ig: impervious ground f_{vg}: fraction of vegetated ground Q_{AH}: anthropogenic heat flux A_{c}: canyon bottom area

Table 3

Urban thermal parameters and tree-related parameters selected for optimization and sensitivity analysis and their respective sampling ranges.

	Descriptions	Minimum	Maximum
Thermal parameters			
α_r / α_w / α_{ig} / α_{vg}	Albedos of roof, wall, impervious ground, and vegetated ground	0.05	0.40 (0.55 for α_w)
ε_r / ε_w / ε_{ig} / ε_{vg}	Emissivities of roof, wall, impervious ground, and vegetated ground	0.80	1.00
C_r / C_w / C_{ig} / C_{vg}	Heat capacities of roof, wall, impervious ground, and vegetated ground (MJ m^{-3} K^{-1})	0.1	2.5
k_r / k_w / k_{ig} / k_{vg}	Thermal conductivities of roof, wall, impervious ground, and vegetated ground (J m^{-1} s^{-1} K^{-1})	0.05	2.50
z_{0r} / z_{0ig} / z_{0vg}	Momentum roughness lengths for roof, impervious ground, and vegetated ground (m)	0.01	0.10
Tree-related parameters			
f_t	Tree fraction	0	1
a_t	Tree-crown radius (m)	1	4
h_t	Tree height (m)	4	10
α_l	Leaf albedo	0.05	0.40
ε_l	Leaf emissivity	0.80	1.00
LAI	Leaf area index	1	6

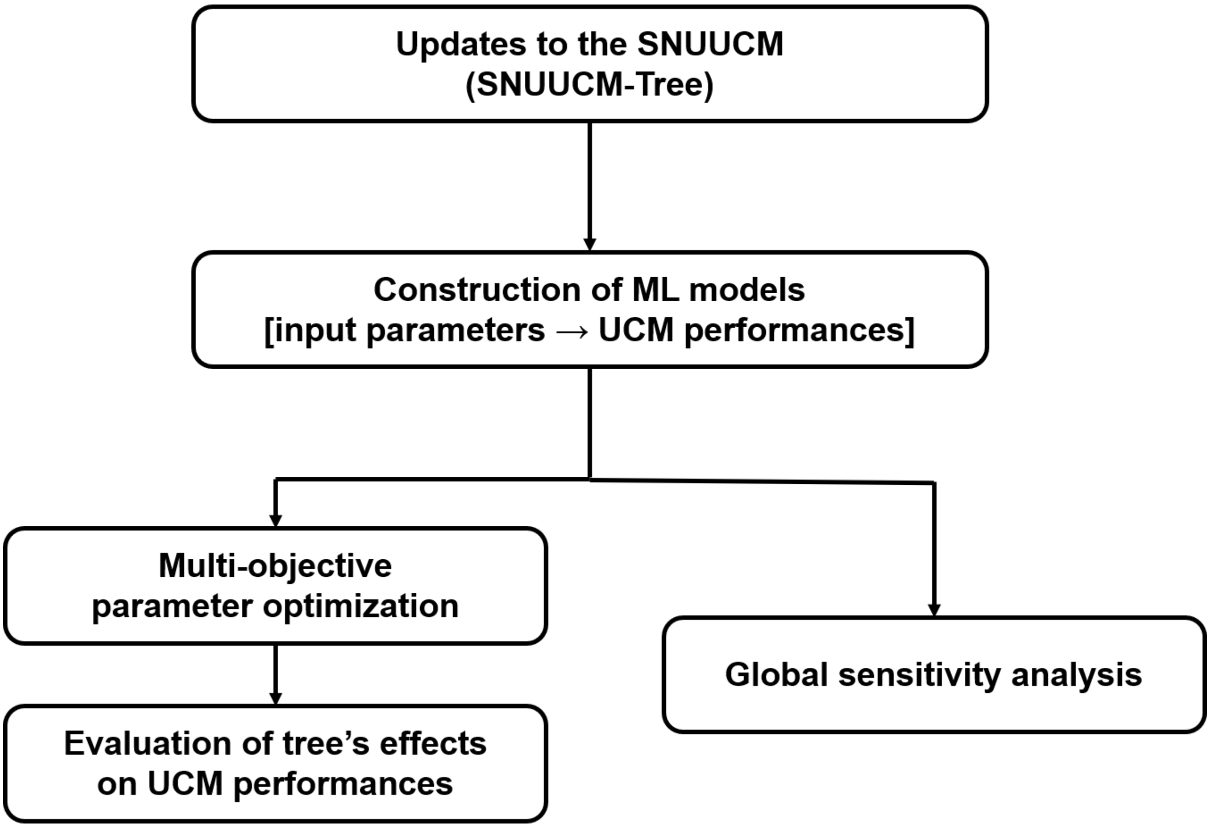

Fig. 1. Overall workflow of this study.

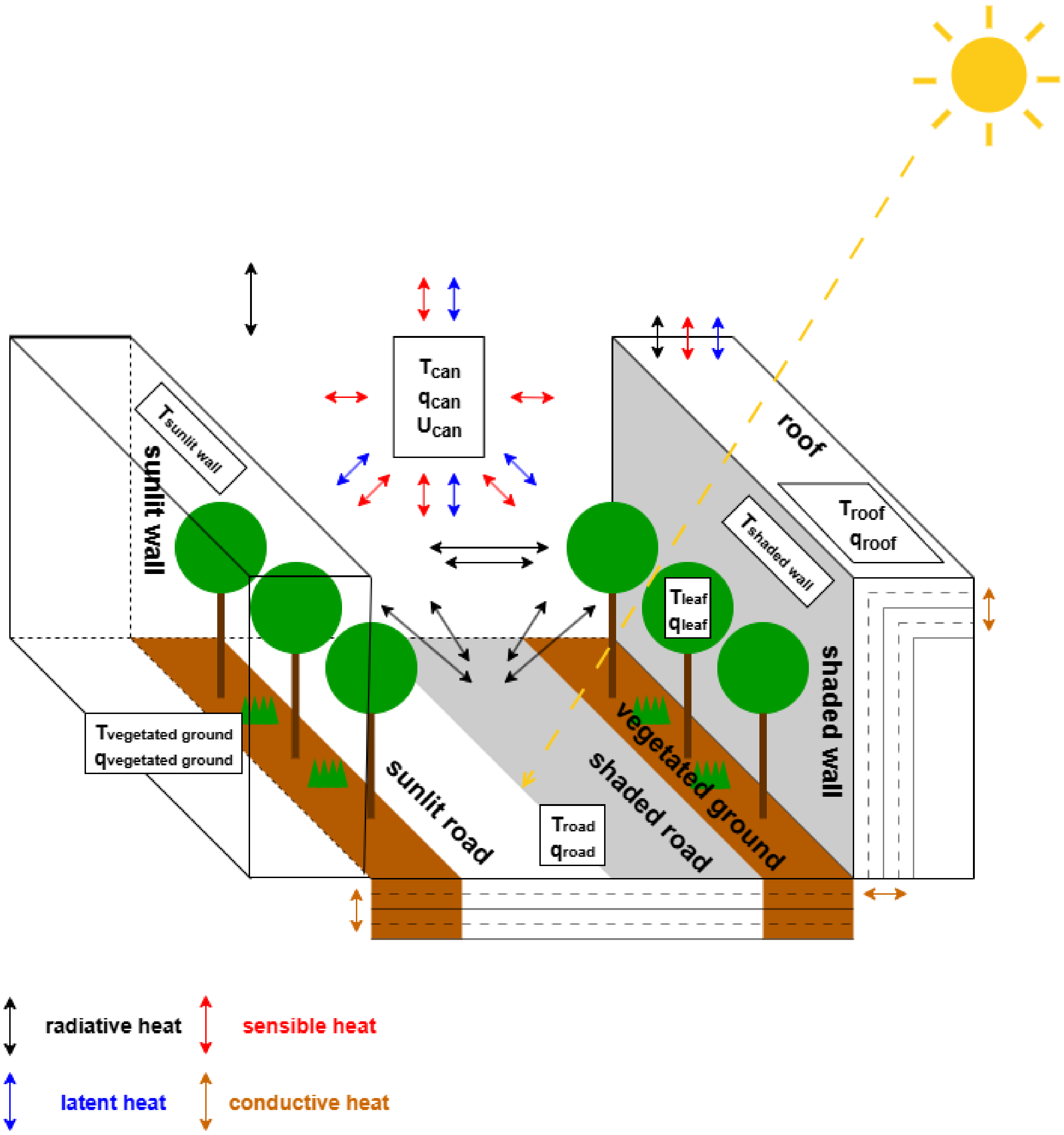

Fig. 2. Schematic diagram of the updated SNUUCM (SNUUCM-Tree).

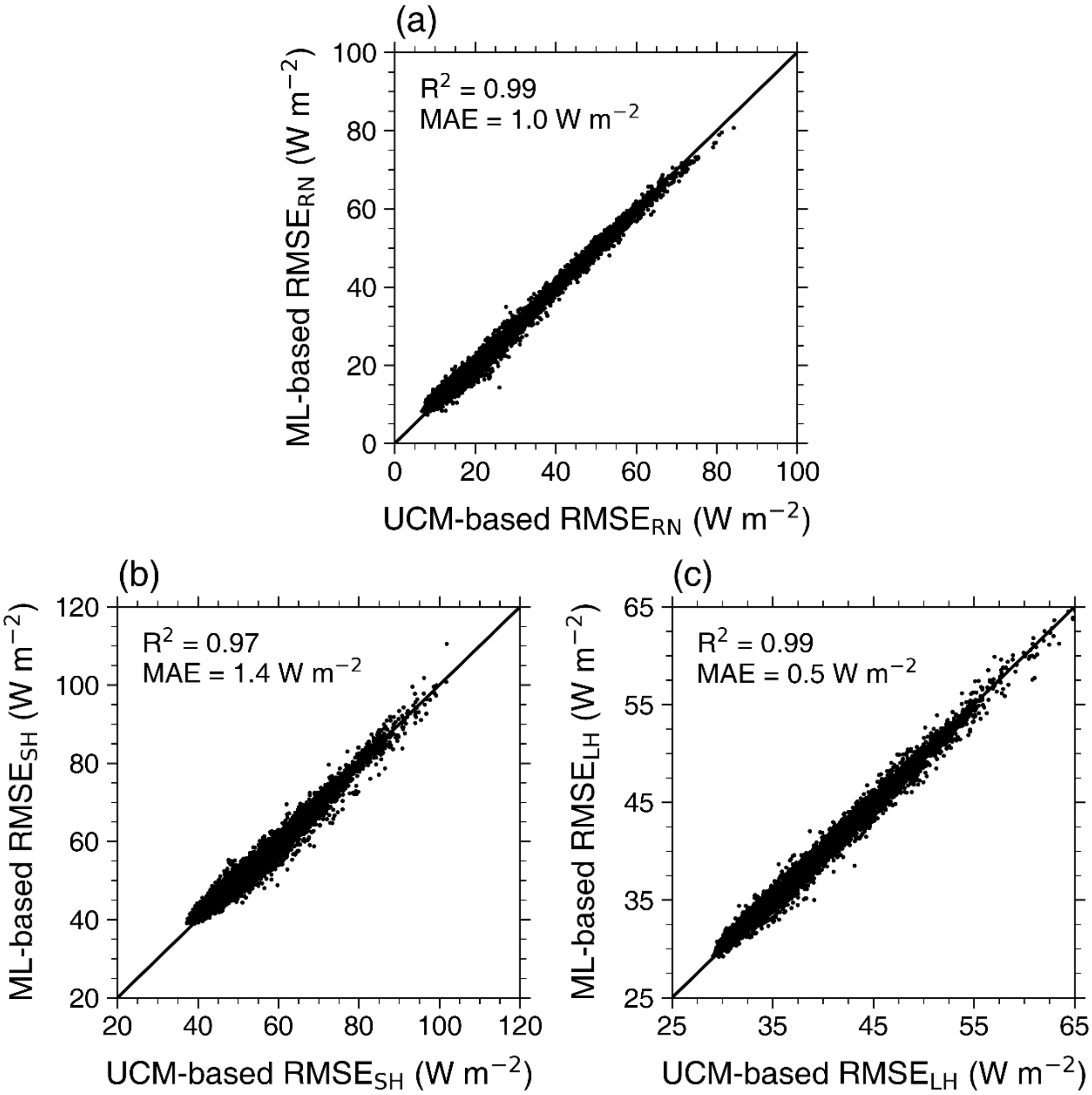

Fig. 3. Scatterplots of the root mean square errors of (a) net radiation ($RMSE_{RN}$), (b) sensible heat flux ($RMSE_{SH}$), and (c) latent heat flux ($RMSE_{LH}$) obtained from the SNUUCM-Tree simulations versus those obtained from the machine learning model simulations.

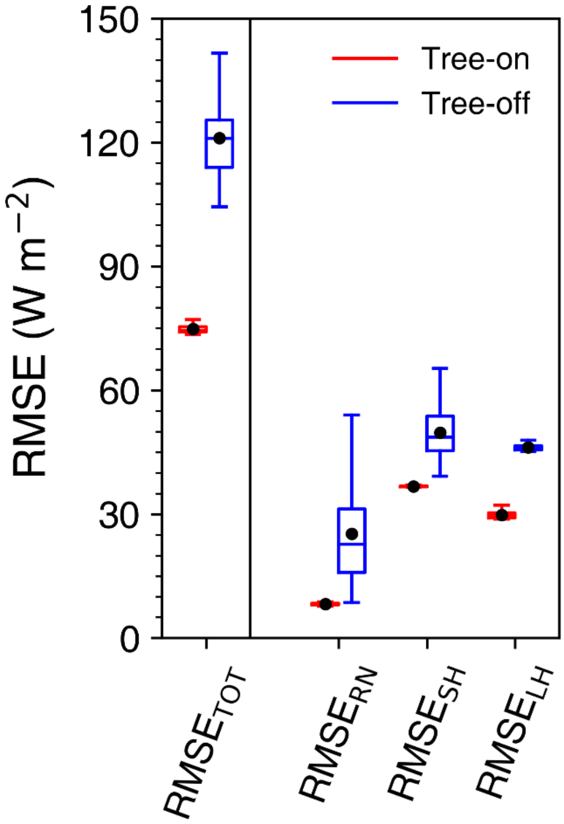

Fig. 4. Box plots of the total root mean square error (RMSE$_{TOT}$) and root mean square errors of net radiation (RMSE$_{RN}$), sensible heat flux (RMSE$_{SH}$), and latent heat flux (RMSE$_{LH}$) obtained from the SNUUCM-Tree simulations with the Pareto-optimal parameter sets in the Tree-on (red) and Tree-off (blue) cases.

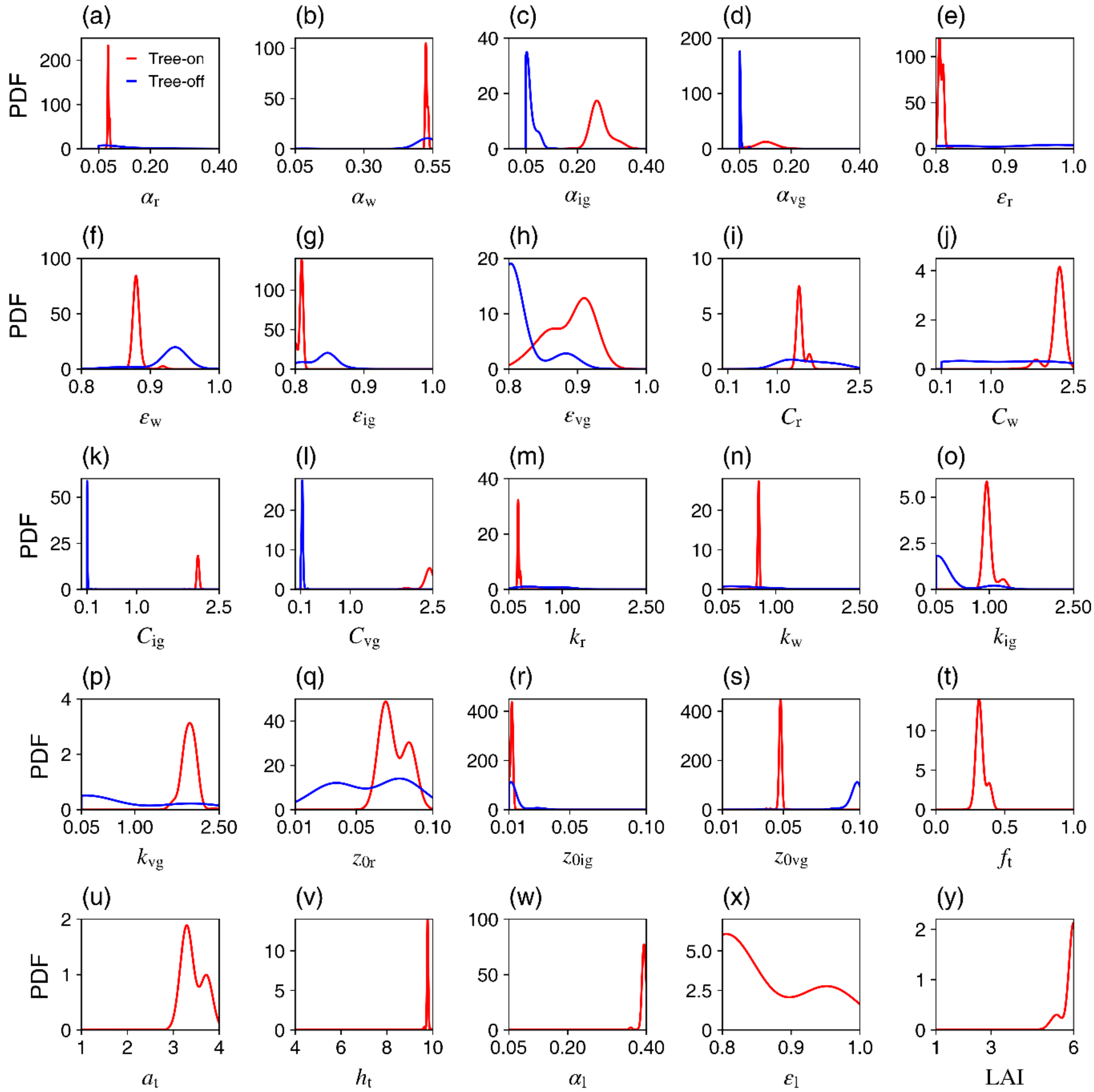

Fig. 5. Probability density functions of the 25 selected input parameters within the Pareto-optimal sets in the Tree-on (red) and Tree-off (blue) cases. The probability density functions of the six tree-related parameters are displayed only for the Tree-on case.

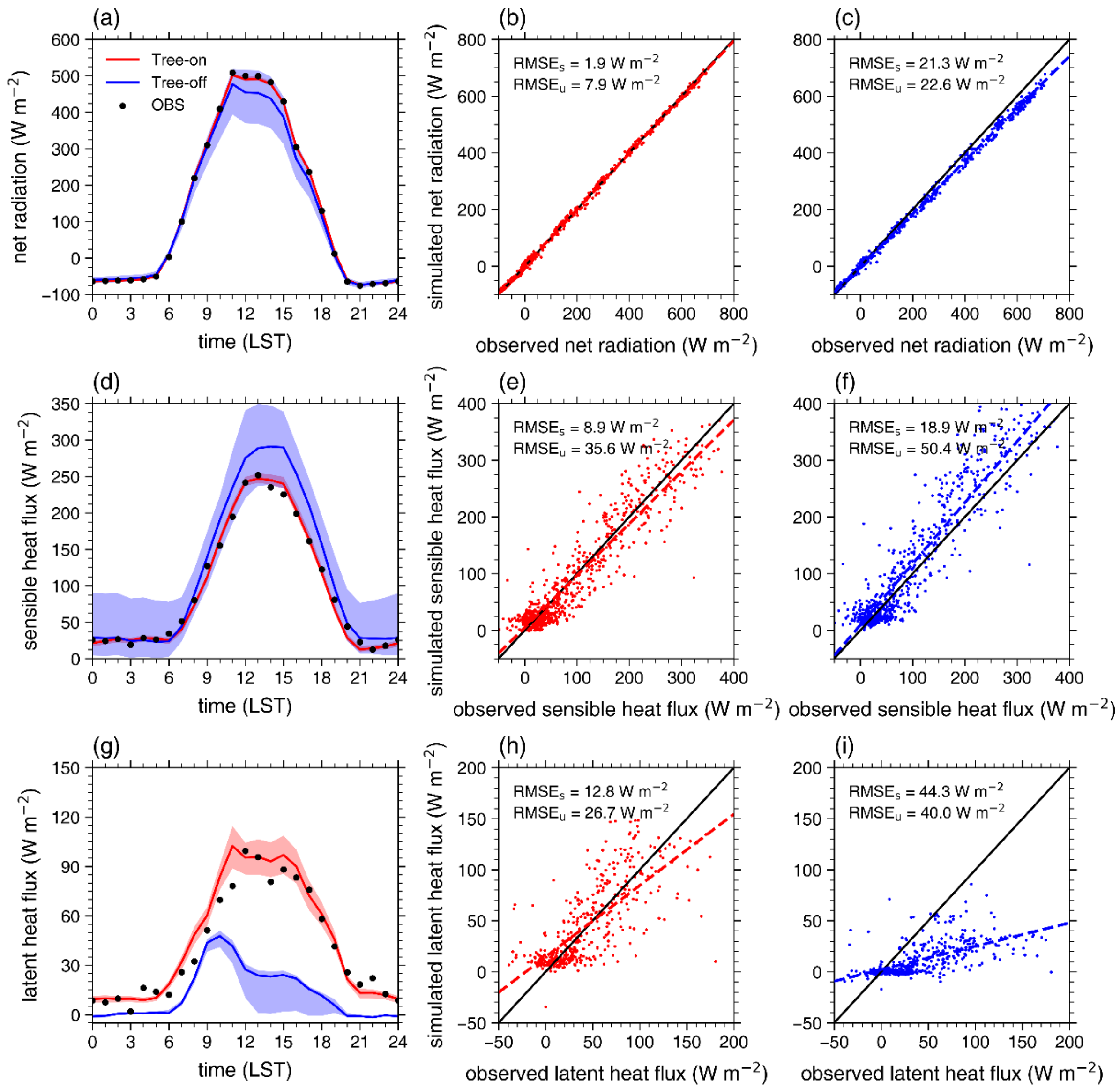

Fig. 6. (a, b, c) Mean diurnal variations of net radiations observed (black dots) and ensemble-averaged over the SNUUCM-Tree simulations with the Pareto-optimal parameter sets in the Tree-on (red solid line) and Tree-off (blue solid line) cases during the analysis period and their scatterplots with the linear regression lines. The spreads of net radiation among the simulations in the Tree-on and Tree-off cases are indicated by light red and light blue shaded areas, respectively. (d, e, f) Same as (a, b, c) except for sensible heat flux. (g, h, i) Same as (a, b, c) except for latent heat flux.

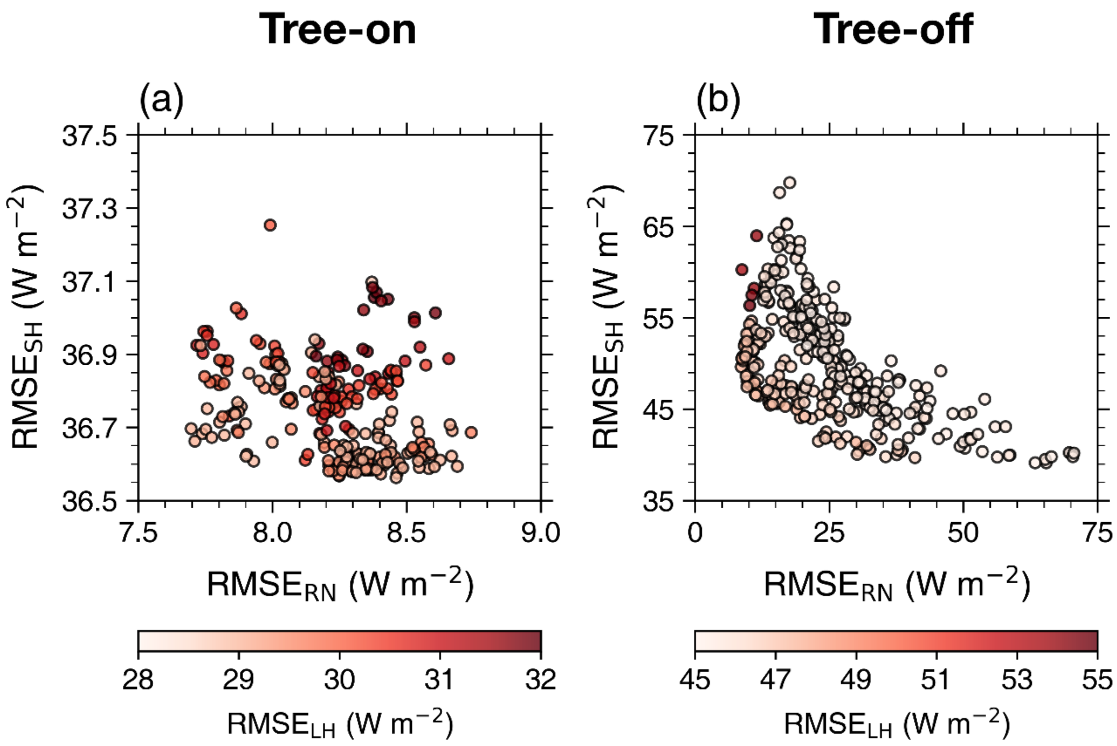

Fig. 7. Scatterplots of $RMSE_{RN}$ versus $RMSE_{SH}$ within the Pareto-optimal sets in the (a) Tree-on and (b) Tree-off cases with $RMSE_{LH}$ colored.

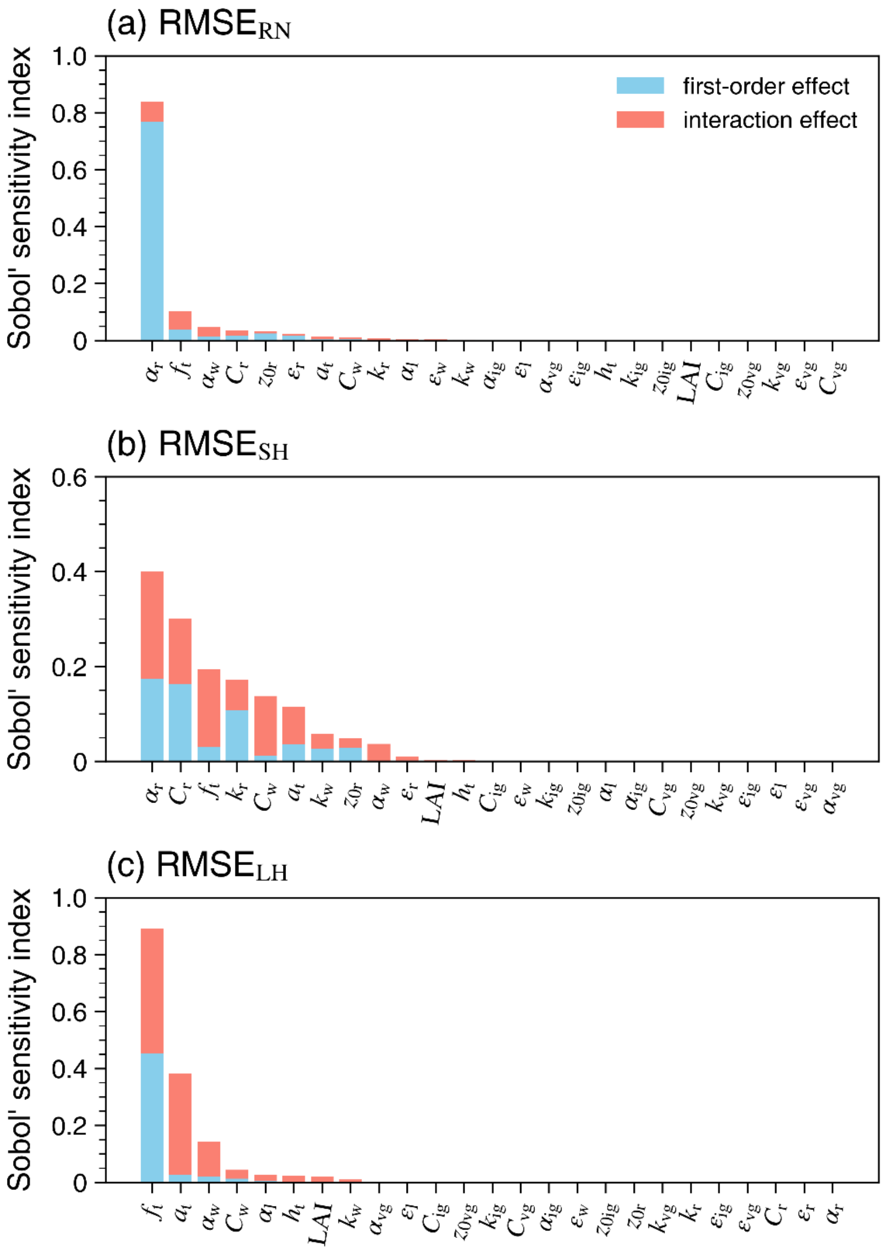

Fig. 8. Bar charts of total-order Sobol' indices of the 25 selected input parameters for (a) RMSE$_{RN}$, (b) RMSE$_{SH}$, and (c) RMSE$_{LH}$ at the Basel-Sperrstrasse site. The first-order and interaction effects are indicated by light blue and light red colors, respectively. The input parameters are arranged in descending order of their total-order Sobol' indices.

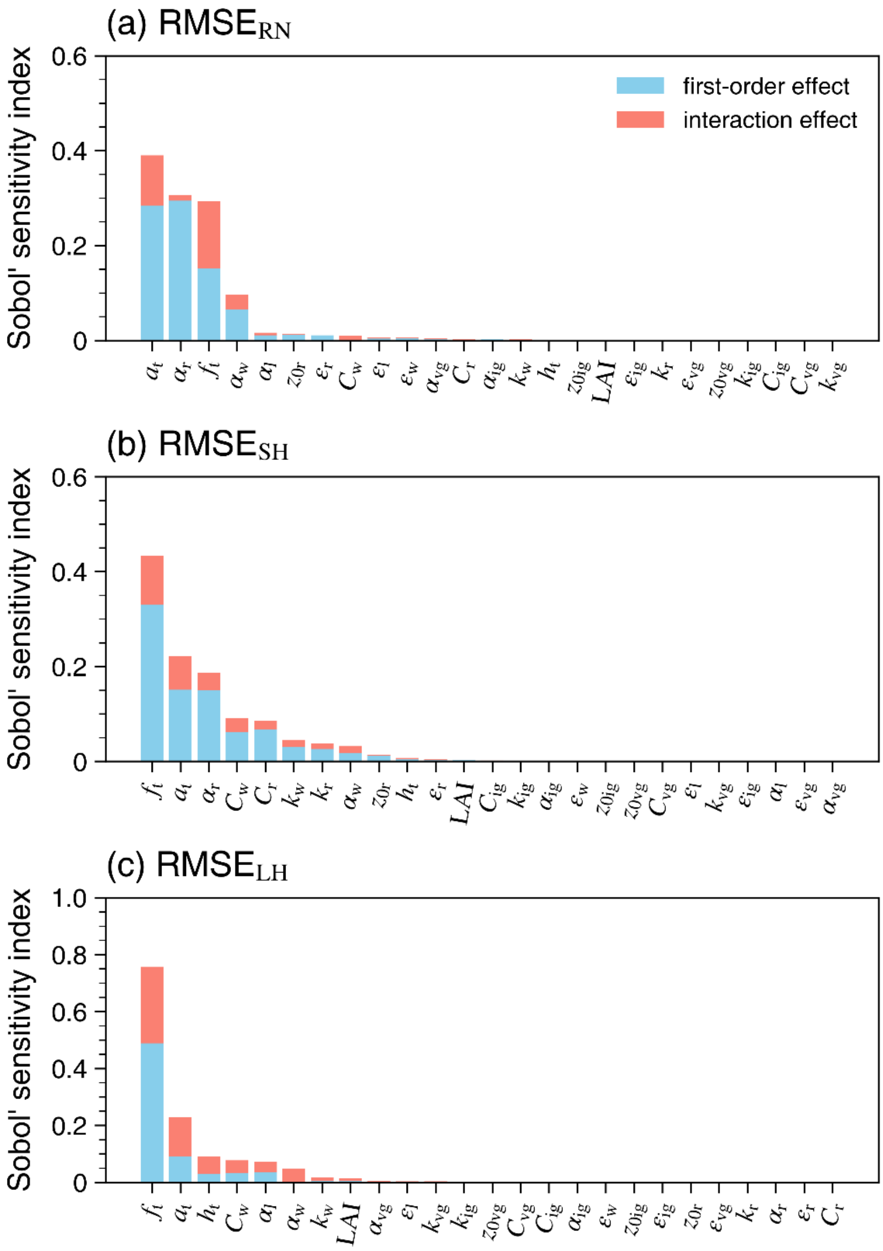

Fig. 9. Same as Fig. 8 except for the Basel-Spalenring site.

Supporting Information for

Evaluating the importance of street trees and their parameters for urban canopy model performance: Model updates and machine learning

Kyeongjoo Park [a], Jong-Jin Baik [a, *], Young-Hee Ryu [b]

[a] School of Earth and Environmental Sciences, Seoul National University, Seoul 08826, South Korea

[b] Department of Atmospheric Sciences, Yonsei University, Seoul 03722, South Korea

[*]Corresponding author:

Prof. Jong-Jin Baik

Email: jjbaik@snu.ac.kr

Table S1

Values of hyperparameters used in the machine learning models for the Basel-Sperrstrasse and Basel-Spalenring sites.

	Basel-Sperrstrasse	Basel-Spalenring
Number of decision trees	1000	984
Maximum tree depth	6	6
Learning rate	0.07	0.04
Subsample ratio	0.64	0.54
Column subsample ratio	0.98	0.98
Minimum loss reduction for splitting	0.005	0.001
L1 regularization	7.30	0.01
L2 regularization	7.91	0.00
Minimum child weight	2.85	1.00

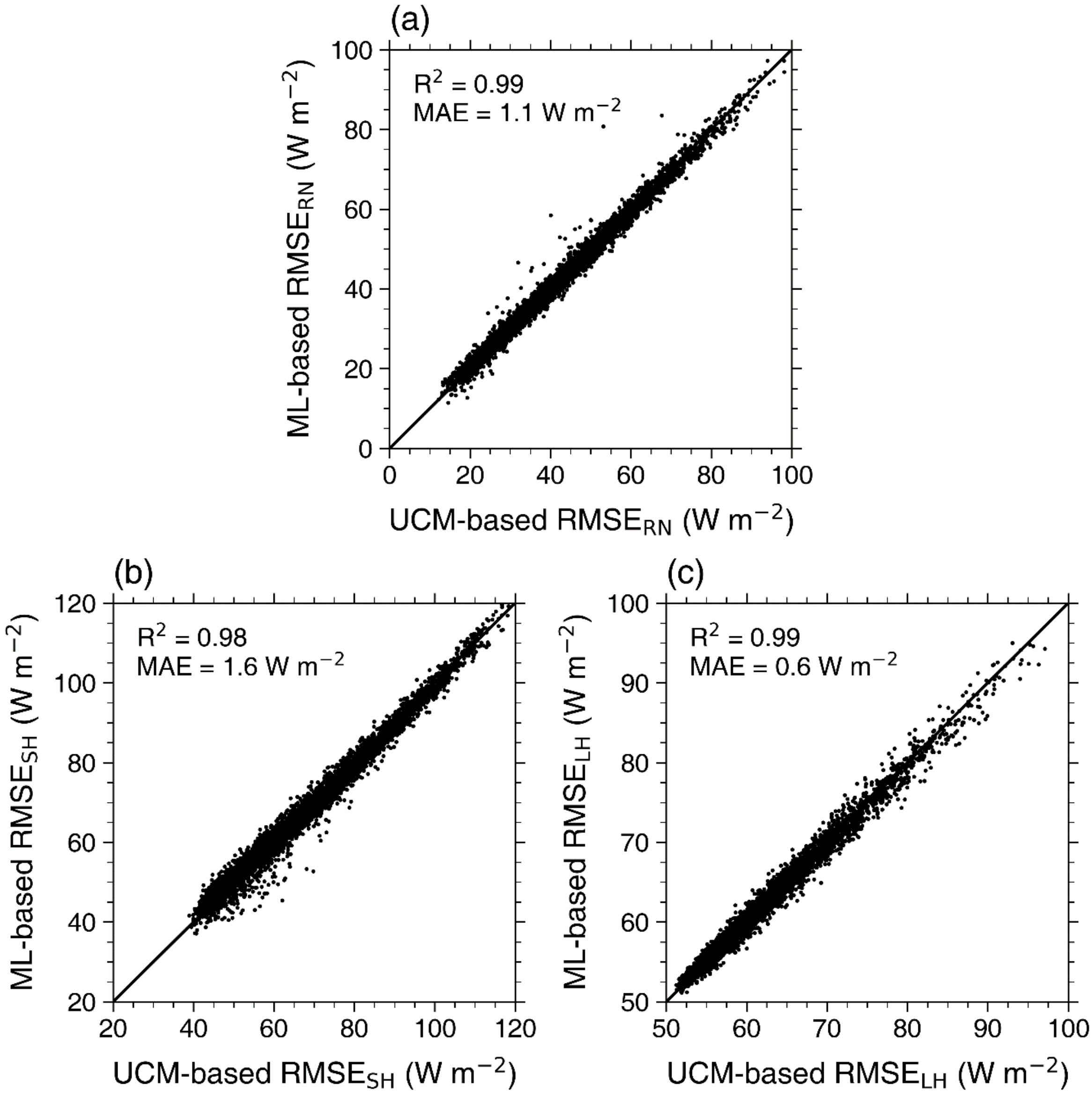

Fig. S1. Same as Fig. 3 except for the Basel-Spalenring site.

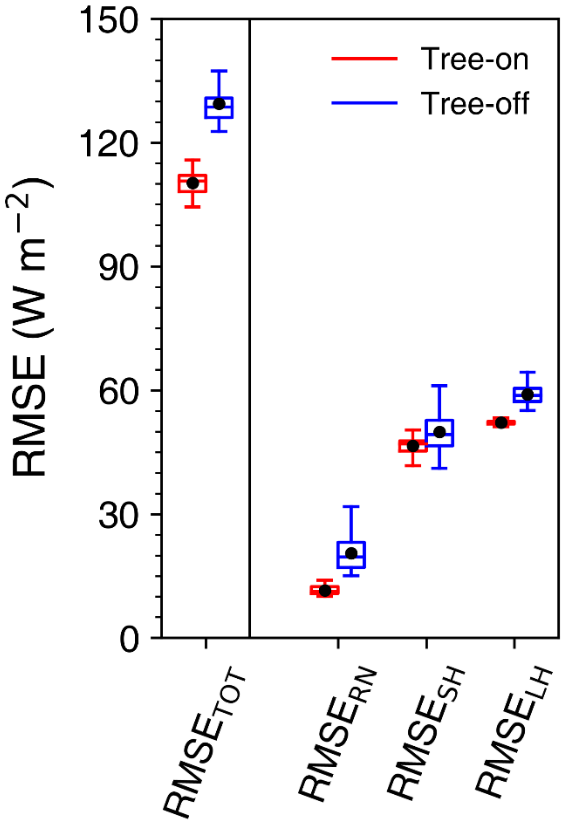

Fig. S2. Same as Fig. 4 except for the Basel-Spalenring site.

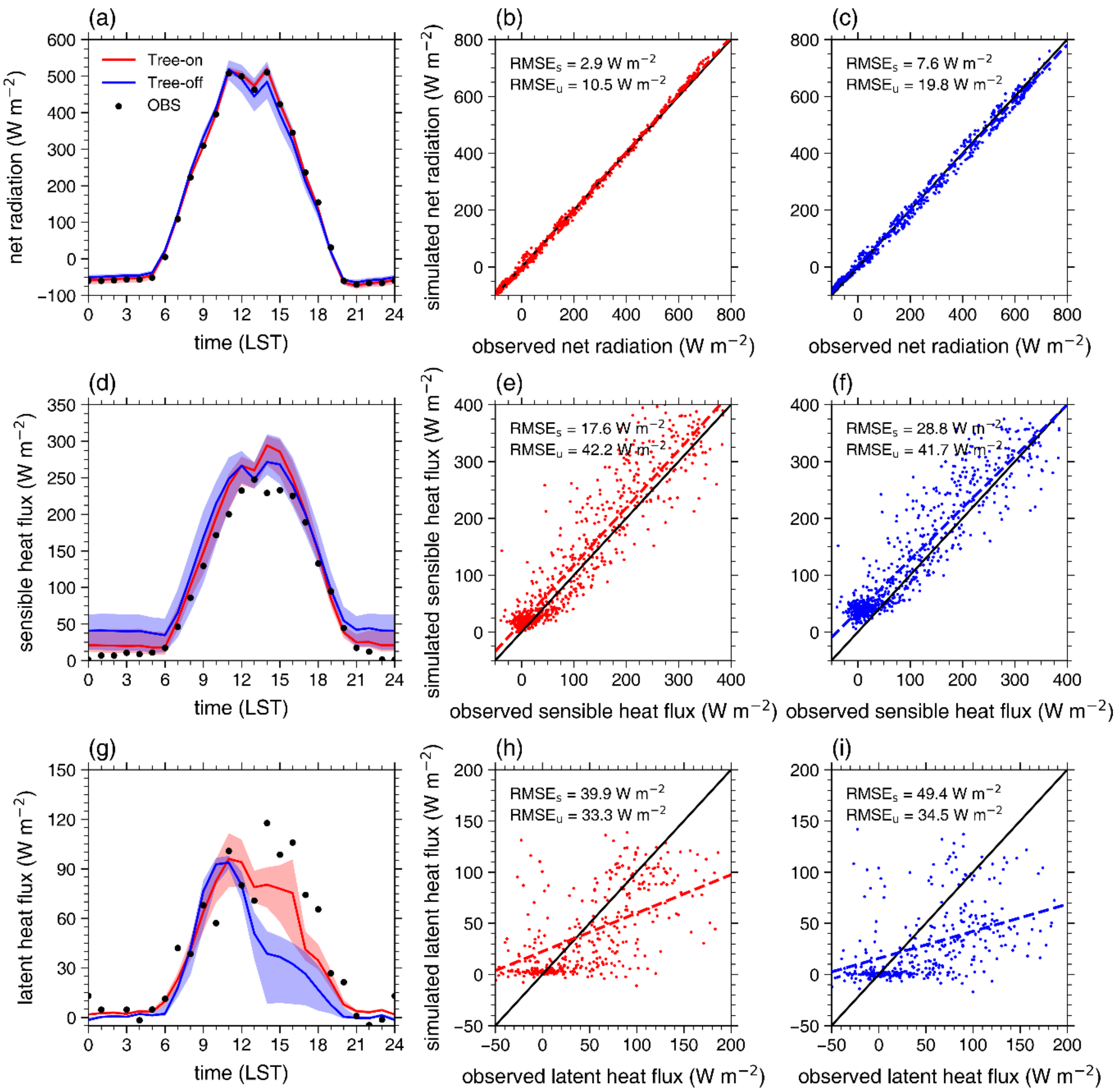

Fig. S3. Same as Fig. 6 except for the Basel-Spalenring site.

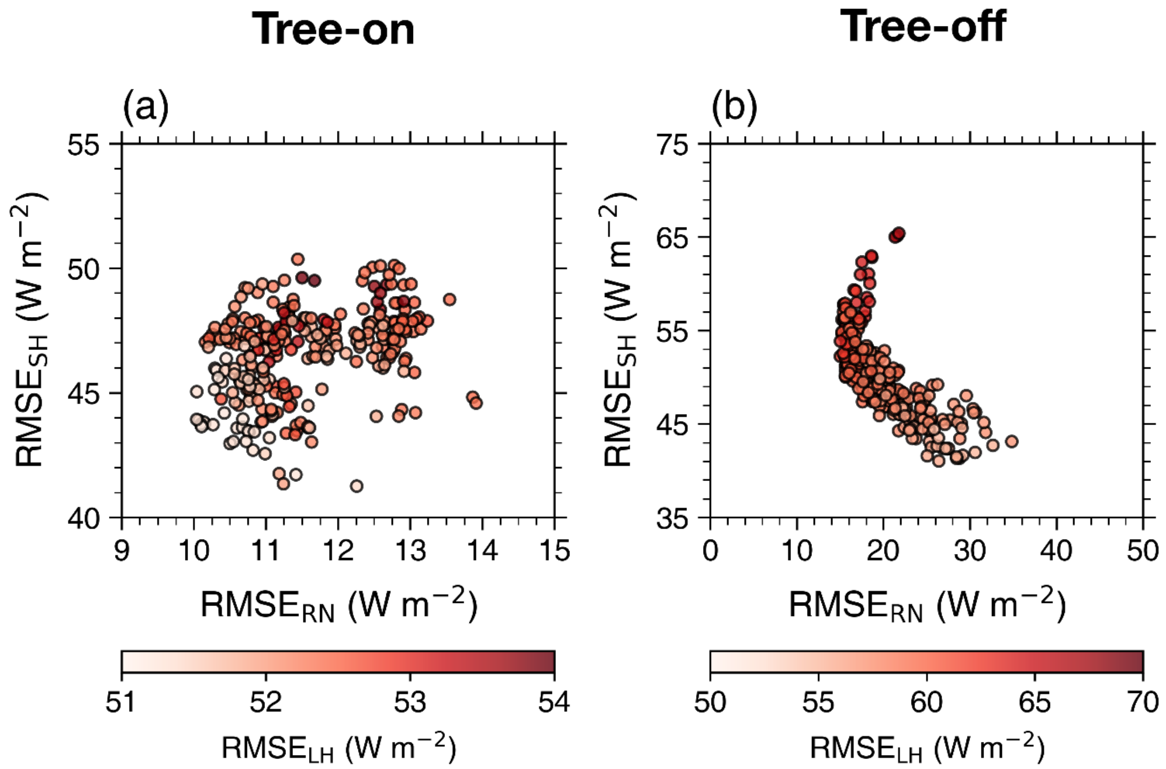

Fig. S4. Same as Fig. 7 except for the Basel-Spalrenring site.